EUROPEAN ORGANIZATION FOR NUCLEAR RESEARCH

ELASTIC AND TOTAL CROSS SECTIONS AND IMPLICATIONS

A.M. Wetherell
CERN, Geneva, Switzerland

Invited talk at the
EPS International Conference on High Energy Physics
Palermo, 23-28 June, 1975

Geneva - 20 August 1975

ELASTIC AND TOTAL CROSS SECTIONS AND IMPLICATIONS

A.M. Wetherell

CERN, Geneva, Switzerland

1. INTRODUCTION

The themes on which I shall mainly concentrate today were much in evidence at the previous European Conference at Aix-en-Provence in 1973. U. Amaldi[1] presented data from the ISR, at that meeting, concerning (i) a rise in the p-p total cross sections of about 10% over the ISR energy range, (ii) an increase towards zero and perhaps a change of sign of the ratio, ρ, of the real to imaginary parts of the p-p forward scattering amplitude in the ISR energy range, (iii) a continuous shrinking of the forward p-p elastic scattering peak, and (iv) the development of a striking structure, akin to a classical diffraction pattern, in p-p elastic scattering.

The discussion of these observations took into account earlier work[2] on points (ii) and (iii) at IHEP (Serpukhov) and suggested some connection of point (i) with the most important result of a rising K^+-p cross section first found[3] at IHEP. Since the Aix-en-Provence meeting the large experimental programme at FNAL has begun to elaborate the picture of hadronic scattering and cross sections suggested by the above facts. Figs. 1 and 2 show the K^+-p and p-p total cross sections[4] as mapped out by the time of the London Conference last year. Furthermore it was found that all hadronic cross sections except for $\bar{p}$-p rise over the energy range of FNAL. In addition, the parameter ρ, for p-p scattering, was found, indeed, to become positive at around 250 GeV and this was linked, on the general grounds of dispersion relations, to the increase of the p-p total cross section. The diffractive-like structure in the p-p elastic angular distribution was further discussed, particularly in the light of geometrical and optical models. Results from FNAL on hadronic elastic scattering up to moderate momentum transfers ($|t| \simeq 1$ GeV^2) appeared, the main effort being devoted to studies of the slope of the diffraction peak. Detailed work on elastic scattering over the whole angular range, typical data[5] being shown in Fig. 3, provided the possibility of studying structures at moderate $|t|$ and backward peaks. Polarization phenomena for various hadrons scattering on polarized protons were pursued up to 45 GeV/c at IHEP and the scattering and interaction of polarized beam protons on polarized target protons has been studied at ANL. Much of this work was reviewed in the report of A.N. Diddens[6] at London last year.

The most recent results which I shall discuss now begin to present a rather coherent picture, in the large, of elastic scattering and total cross sections. The framework for its discussion remains phenomenological, containing such elements as geometrical models, quark and parton considerations and Regge features. Dispersion relation and analyticity approaches also play an important role and evidently provide useful tools in discussing experimental data, although how powerful such machinery is provides a basis for continuing discussion.

2. TOTAL CROSS SECTIONS

2.1 ISR Measurements

The collaboration of Aachen-CERN-Heidelberg-Munich has measured[7] the p-p total cross section at five energies between 23.6 and 62.8 GeV in the c.m.s. The method used was the same as that previously employed[8] by the Pisa-Stonybrook group, namely a determination of the total interaction rate and of the machine luminosity. Scintillation counter hodoscopes picked up ≃ 90% of the interactions and a streamer chamber detected event topologies missed by the hodoscopes. The results are given in table 1 together with the published data of the CERN-Rome[9] and of the Pisa-Stonybrook[8] groups. The new data exhibit an increase of about 10% over the ISR energy range in good agreement with the previous experiments.

Table 1

ISR p-p total cross sections

$\sqrt{s}$ (GeV)	σ_T (ACHM) a) (mb)	σ_T (PSB) b) (mb)	σ_T (CR) c) (mb)
23.6	38.7 ± 0.7	39.3 ± 0.8	39.1 ± 0.4
30.8	40.0 ± 0.6	40.9 ± 0.8	40.5 ± 0.5
45.2	42.5 ± 0.8	42.6 ± 0.9	42.5 ± 0.5
53.2	42.9 ± 0.7	43.0 ± 0.8	43.2 ± 0.6
62.8	44.1 ± 0.9	44.0 ± 0.8	

a) ACHM is Aachen-CERN-Heidelberg-Munich
b) PSB is Pisa-Stonybrook
c) CR is CERN-Rome. (An overall systematic error of ± 0.6 mb should be included in the CR results.)

2.2 FNAL Measurements

General Discussion

The experiment at FNAL, Carroll et al. (BNL, FNAL, Rockefeller), which demonstrated the essential universality of rising hadronic cross sections, has been continued[10] to momenta of 280 GeV/c. The technique was that of a very refined transmission measurement in which cross sections for $\pi^{\pm}$, $K^{\pm}$, p and $\bar{p}$ interactions with protons and deuterons were obtained at 11 beam momenta between 23 and 280 GeV/c. Results for hadron-proton interactions are shown in Fig. 4, which exhibits that all of the cross sections, except K^+, decrease with increasing momentum, pass through shallow minima and then increase, except for $\bar{p}$ where there is no rise up to 200 GeV/c. However, it would appear to be natural to expect that the $\bar{p}$-p cross section will rise at momenta greater than so far explored. That the $\bar{p}$-p cross section should always be larger than that for the p-p system would

appear to be a somewhat reasonable intuition, as there should always be more reaction channels open for $\bar{p}$-p than for p-p. The possible trend for $\bar{p}$-p will be considered later. Fig. 5, for the deuteron target, shows the same features as Fig. 4 together with a nice (and necessary) demonstration of charge symmetry for strong interactions, whereby $\sigma(\pi^- d) = \sigma(\pi^+ d)$. In fact, averaging over the data presented, the ratio of the latter cross sections is 1.0014 ± 0.0009. Cross sections for a neutron target were obtained from the hydrogen and deuteron data using the usual Glauber-Wilkin[11] incantation. The radius parameter $\langle r^{-2} \rangle$ was obtained from the π-p and π-d cross sections and a summary of results is given in Fig. 6, showing, for the new data, a momentum independent value averaging to 0.039 mb^{-1}. This value has been used for kaons but for protons and anti-protons a value of 0.035 mb^{-1} was employed as a consequence of discussions[4] on whether or not $\langle r^{-2} \rangle$ is dependent upon the particle concerned. It should be noted that an uncertainty of ±0.004 mb^{-1} in $\langle r^{-2} \rangle$ leads to an uncertainty of ±1.5% in the p-n cross section and ±0.7% in the K-n cross section. Fig. 7 presents the data on target neutrons so obtained, the dotted curves representing the limits of the p-n cross section for $\langle r^{-2} \rangle$ between 0.039 and 0.031 mb^{-1} .

While the overall picture of the target neutron cross sections reflect well the behaviour of the target protons, several more detailed remarks are in order concerning the p-n cross section. First, the recent measurements of n-p cross sections, by Longo et al.[12], using a neutron beam and hydrogen target are in agreement with the p-n data above 80 GeV/c. Secondly there is some discrepancy between the p-n data of Denisov et al.[3,13] and the FNAL experiment between 35 and 65 GeV/c. This is unfortunate as the difference of the iso-triplet and iso-singlet nucleon-nucleon cross sections, Fig. 8, puts constraints on the behaviour of p-n charge exchange scattering and, in any case, crossing points of total cross sections have general interest. At the moment I would say that the situation of high energy crossovers of the nucleon-nucleon cross sections is obscure. At the highest energies, however, the p-p and p-n cross sections seem at face value to be converging following the Okun-Pomeranchuk rule[14] for particles of the same iso-multiplet. The difficulties of reaching firm conclusions on the differences of p-p and p-n cross sections have been underlined by Leader and collaborators[15] and the subject seems, as often before, to deserve further experimental and theoretical study.

2.3 Cross Section Relationships

The difference between cross sections for antiparticles and particles are expected to approach zero and the way in which this occurs contains useful information. Fig. 8 shows these trends as functions of momenta, the cross section differences exhibiting, very well, a power law dependence. The fits shown in Fig. 8 are of the Regge form $\sim s^{\alpha-1}$ and the values of α obtained are given in table 2. It may be observed that a value of $\alpha \simeq 0.4$ is common for all particle systems apart from π-p, which is described by a value of 0.55. The latter lies close to the $t = 0$ intercept of the ρ trajectory and indeed the $\pi^{\pm}$-p total cross section differences agree within errors with the predictions from the forward charge exchange results of Barnes et al.[16].

Table 2

Fit $\Delta\sigma = \sigma_T(\bar{x}\text{-}t) - \sigma_T(x\text{-}t) \sim s^{\alpha-1}$

x	t	α
p	p	0.39 ± 0.02
p	d	0.40 ± 0.02
p	n	0.39 ± 0.04
K	p	0.40 ± 0.04
K	d	0.41 ± 0.03
K	n	0.38 ± 0.11
π	p	0.55 ± 0.03

Using the power law for the $\bar{p}$-p, p-p cross section difference one can extrapolate the $\bar{p}$-p cross section, the result being shown in Fig. 9. The indications are that a considerably higher energy or increased experimental precision will be needed to observe a significant rise in the $\bar{p}$-p cross section.

The combinations of cross sections and their differences provide insight into the validity of strong exchange degeneracy and universality for the leading Regge exchanges. The necessary relationships are summarized in the paper of Hendrick et al.[17]. Fig. 10 exhibits the situation for ω and for ρ-ω universality, the ratios indicated being reasonably well distributed about the value unity. Fig. 11 compiles the data for A_2 universality which is perhaps rather less well satisfied.

The Levin-Frankfurt[18] rule for quark addition may also be examined.

Defining

$$\bar{\sigma}\,(\pi N) = \tfrac{1}{2}\{\sigma\,(\pi^+ p) + \sigma\,(\pi^- p)\}$$

$$\bar{\sigma}\,(KN) = \tfrac{1}{4}\{\sigma\,(K^+ p) + \sigma\,(K^- p) + \sigma\,(K^+ n) + \sigma\,(K^- n)\} \qquad (1)$$

$$\bar{\sigma}\,(NN) = \tfrac{1}{4}\{\sigma\,(pp) + \sigma\,(\bar{p}p) + \sigma\,(pn) + \sigma\,(\bar{p}n)\}$$

$$R_1 = \frac{2}{3}\frac{\bar{\sigma}\,(NN)}{\bar{\sigma}\,(\pi N)} \qquad (2)$$

$$R_2 = \frac{\bar{\sigma}\,(\pi N)}{\bar{\sigma}\,(KN)} \qquad (3)$$

Fig. 12 shows the tend of R_1 and R_2 with momentum. The data exhibit a slow decrease of R_1 and R_2 towards unity as expected on the basis of the simple additive quark model[18]. Clearly if this trend continues this quark limit will be attained at some incredibly high energy!

Finally the Johnson-Treiman[19] relations may be tested and this is done in Figs. 13 and 14. There is a suggestion of some systematic deviation occurring at high energy in Fig. 13. The data of Fig. 14, however, are inconclusive, the problems of a neutron target once more causing difficulties.

2.4 Cross Section Trends

Having discussed, superficially, the details of the high energy cross sections, what may be said about their overall behaviour? Morrison[20] has remarked that, in fact, the p-p total inelastic cross section rises monotonically above about 6 GeV/c with a power law $\sim s^{0.04}$, the minimum in the total cross section arising from an interplay between a decrease of the total elastic cross section at low energies and the continuous rise of the inelastic. A more recent observation concerning the K^+-p cross section has been made by Goulianos[21]. Some sort of two component description therefore appears to be indicated.

With regard to the rate of rise of the cross sections it can be said immediately that the observed rate of increase is well within the Froissart bound[22].

$$\sigma_T < \frac{\pi}{m_\pi^2} \left(\ln \frac{s}{s_0}\right)^2 \tag{4}$$

the constant in front of the logarithm being about 62 mb, and $s_0 = m_\pi^2$. That the present situation is very far from this is illustrated by a simple fit for the NAL and ISR data for p-p namely:

$$\sigma_T\,(pp) = 38.24 + 0.376 \left(\ln \frac{s}{93.71}\right)^{2.1} \tag{5}$$

and by a similar fit to the NAL K^+-p data

$$\sigma_T\,(K^+p) = 17.25 + 0.37 \left(\ln \frac{s}{20}\right)^{1.82} \tag{6}$$

Successful detailed fits[23] to last year's data were reported at the London Conference. They are of the two component form

$$(\bar{\sigma}-\sigma) = 2\sigma_2 E^{-\alpha_2} \tag{7}$$

$$(\bar{\sigma}+\sigma) = 2\,(\sigma_1 E^{-\alpha_1} + \sigma_\infty) \tag{8}$$

where σ and $\bar{\sigma}$ are the total cross sections for particle and antiparticle on protons, respectively. The two terms $\sigma_i E^{-\sigma i}$ are suggested by Regge ideas. For the asymptotic cross section, σ_∞, three parametrizations were tried:

$$\sigma_\infty = \sigma_0 \left(1+C(\ln\gamma)^2\right) \tag{9}$$

$$\sigma_\infty = \sigma_0 \ln\gamma \tag{10}$$

$$\sigma_\infty = \sigma_0 \gamma^{\alpha 0} \tag{11}$$

In the latter the parameters C and σ_0 are the same for all the particle combinations and γ is the particle Lorentz factor. These fits remain essentially valid for the new data. Extensive work in this domain has been done more recently by Hendrick et al[17] on a similar basis to the work of Bartel and Diddens[23], with Regge phenomenology firmly embedded in the fits. Figs. (1) and (2) in fact show fits of Hendrick et al., they use:

$$\sigma_T(K^+p) = 3.27\left(\ln \frac{p+1.49}{0.80}\right) \tag{12}$$

$$\sigma_T(pp) = 4.91\left(\ln \frac{p+541}{0.30}\right) + 11.1p^{-0.58} \tag{13}$$

where the cross section units are millibarns and p is the laboratory momentum in GeV/c. It is concluded that with the present data the functional form of the rising cross sections is undetermined. Clearly either higher energies or other information is needed to make progress on this question.

A simple view of a two component description of total cross sections is given by a consideration of Lipkin[24]. Taking as a parametrisation the sum of a decreasing Regge part, R, and a slowly varying component f

$$\sigma_T(s) = Rs^{-\frac{1}{2}} + f(s) \tag{14}$$

so that at high energies

$$\sqrt{P}_{Lab}\ \sigma_T(s) \sim R + \sqrt{P}_{Lab}\ f(s) \tag{15}$$

Fig. 15 shows $\sqrt{P}_{Lab}\sigma_T$ plotted against $\sqrt{P}_{Lab}$ with the quark counting coefficients of 2/3 applied to the baryon cross sections. The picture gives a nice impression of orderliness and further analysis along these lines should provide more insight into the Regge term splitting between the cross sections and perhaps of the rise itself, the suggestion[25] of a "two component Pomeron" having already been made.

2.5 Cross Sections of Vector Particles

The universal rise of hadron cross sections leads to the question as to whether or not the photon-proton cross section will rise from its present plateau of $\simeq$ 120 ub. The present data[26], Fig. 16, are at too low an energy, but during the next year an FNAL experiment should be studying the γ-p cross section up to $\sim$ 200 GeV. A related question

is that of the cross sections of vector mesons. Photoproduction data and application of the vector dominance model (VDM) relations and a diffractive assumption yield vector-meson-proton total cross sections as follows:

$$\frac{d\sigma}{dt}(\gamma p \to Vp) = \frac{3\Gamma}{\alpha m_V}\frac{d\sigma}{dt}(Vp \to Vp) = \frac{3\Gamma}{16\pi\alpha m_V}\left[\sigma_T(Vp)\right]^2 e^{Bt} \qquad (16)$$

where m_V is the meson mass, Γ its partial width for decay to e^+e^- and B the V-p elastic scattering slope parameter. Results obtained in this way by Barger and Phillips[27] are given in Fig. 17 which shows cross sections for ρ-p and ϕ-p. The values are large and hadronic as, of course, they should be. Photoproduction[28] of the $\Psi(3095)$ has been discussed in another session[29]. A summary of the Ψ-p total cross section deduced from the data by Barger and Phillips[30] is given in Fig. 18. This shows cross sections obtained by standard vector meson dominance and by taking into account kinematical flux factors necessitated by the difference between photon and vector meson masses. Here it suffices to note that the high energy Ψ-p cross section is about 1 mb leading to the identification of the Ψ as a hadron.

3. ELASTIC SCATTERING

3.1 Small Angle Region ($|t| \leq 10^{-2}$ GeV^2)

The measurement of very small angle scattering, where Coulomb effects are significant, provides a means of measuring the ratios of real and imaginary parts of the scattering amplitude, Coulomb interference providing an absolute phase determination. As is well known, the real part of the scattering amplitude is related to the absorptive part, or total cross section, by means of a dispersion relation. Rigorous investigations of dispersion relations by Khuri and Kinoshita[31] have shown that constant total cross sections imply $\rho = 0$, rising σ_T imply $\rho > 0$ and for falling σ_T $\rho < 0$. In addition, for any rise of σ_T slower than the lab energy E, ρ falls to zero from above as $E \to \infty$, provided that the differences of particle and anti-particle cross sections tend to zero. Other theoretical apparatus in the shape of derivative analyticity relations[32] relate ρ and the behaviour of σ_T. A simplified and transparent relation for the scattering amplitude, F, which results[33] is

$$\mathrm{Re}\ F \simeq \frac{\pi}{2}\frac{d\sigma_T}{d\ln s} \qquad (17)$$

Hence high energy rising cross sections must necessarily be accompanied by positive ρ. It is clear then, that, either by means of normal dispersion relations or by the analyticity approach, information on ρ at some fixed energy gives some guide as to the behaviour of σ_T at higher energies. With these remarks in mind I shall now discuss data on the parameter ρ for the six stable particle configurations. The data is presented in the framework of dispersion relation evaluations of Hendrick and Lautrup[34]. Their calculations of ρ were performed using the previous data of Carroll et al.[4] and recent determination of the

subtraction constants, coupling constants and unphysical cut contributions to the dispersion relations. The cross section used above the presently available energies were those derived from the fits[17] mentioned in section 2.4. The shaded regions in the graphs to be shown represent the calculated range of values caused by uncertainties in the total cross section measurements and in the dispersion relation parameters.

Fig. 19 shows the present situation for p-p scattering, the FNAL data from Bartenev et al.[35] demonstrating a zero at around 250 GeV/c and positive real part values above, as suggested by the ISR data of Amaldi et al.[36]. A new and preliminary data point from the FNAL-Yale group[37] is shown at 70 GeV/c and is in good agreement with the general trend. In terms of potential language Fig. 19 indicates that at low energies the nucleon-nucleon face is attractive, then repulsive and then once more attractive above 250 GeV.

Fig. 20 gives the status of ρ for $\bar{p}$-p scattering. New data from the CERN PS at low energies is presented by Jenni et al.[38] and falls neatly along the dispersion relation prediction. A preliminary value at 70 GeV/c from FNAL-Yale [37] suggests that there is a zero a little below 100 GeV/c, around the predicted value.

Fig. 21 presents π^+-p data and in particular a preliminary value of FNAL-Yale [37] at 70 GeV/c indicating a zero in that region. The new point ties down nicely a rather open situation beyond the data of Baillon et al.[39] and Foley et al.[40].

Fig. 22 shows ρ for π^--p, the IHEP data of Apokin et al.[41] up to 59 GeV/c indicating a zero in the neighbourhood. The new, preliminary point from FNAL-Yale[37] at 70 GeV/c tends to support this.

Fig. 23 gives the data available on K^+-p scattering the preliminary value at 70 GeV/c from FNAL-Yale[37] suggesting a zero somewhat below 100 GeV/c. The experimental situation is, however, clearly not very good and deserves much more attention.

Fig. 24 indicates a rather confusing situation for K^--p scattering. The low energy data points of Baillon et a.[42] were obtained electronically, the three higher energy points by bubble chamber measurements[43] and the preliminary highest energy point at 70 GeV/c by FNAL-Yale[37] using their multiwire proportional chamber spectrometer. The value for ρ at 14.3 GeV/c, from the Amsterdam-Nijmegen-Ecole Polytechnique collaboration, has recently been revised[44], as indicated.

To summarize, it appears that, apart from the K^--p situation, a rather consistent picture relating ρ and σ_T is emerging with positive trends for ρ relating to rising σ_T. Further work from the FNAL-Yale group at other and higher energies will help to fill in this picture and a new experiment at the ISR by the CERN-Rome collaboration[45] will attempt to measure ρ, for p-p collisions at momenta corresponding to 2000 GeV/c in the laboratory system. If successful this measurement may help to indicate the trend of the proton-proton cross section at energies higher than 2 TeV.

3.2 Diffraction Peak Region

3.2.1 Summary

The data to be discussed are summarized in table 3.

Table 3

Group	Particles	Momentum Range (Gev/c)	$\|t\|$ Range GeV^2	Structure
Karlsruhe-ITEP (Moscow)	n-p	10-70	0.1-2.8	Kink around $\|t\| = 1.3$ GeV^2
IHEP- (Serpukhov)	π^+, K^+, p	29-65	0.08-1.0	
Michigan-ANL-FNAL-Indiana	$\pi^\pm$, $K^\pm$, $p^\pm$	50-200	0.08-1.0 but larger for K^+, p, π^-	at 200 GeV in p-p dip at $\|t\| \simeq 1.5$ GeV^2; kink in π^- at 200 GeV, $\|t\| \simeq 0.4$ GeV^2?
SASF (at FNAL)	$\pi^\pm$, $K^\pm$, $p^\pm$	50-175	0.04-0.8	
CHOV (ISR)	P	290 and 2100	0.03-3.5 0.21-3.5	minimum around $\|t\| \simeq 1.3$ GeV^2

3.2.2 Forward Peak

The single arm spectrometer facility (SASF) group present data[46] on the forward peak in terms of the fit

$$\frac{d\sigma}{dt} = A\exp(-B|t| + Ct^2) \tag{18}$$

and adopt as a slope parameter b_e, given by

$$b_e = B + 2C|t| \tag{19}$$

where $|t| = 0.2$ GeV^2

Fig. 25 summarises their data, together with the IHEP results of Antipov et al.[47]. The energy dependence of b_e weakens as the energy increases and the $\bar{p}$-p and p-p trends are converging.

The SASF group should, in due course, be able to study in detail the region around $|t| \simeq 0.15$ GeV^2 where there is an apparent change of slope in p-p data[48] from the ISR.

The Michigan-ANL-FNAL-Indiana collaboration (Akerlof et al.) present data[49] on the slope parameter b obtained from a simple exponential fit and the total elastic cross section σ_{el}. At 200 GeV/c the ratio of σ_{el}/σ_T is about 0.145, 0.142 and 0.193 for $\pi^{\pm}$-p, $K^{\pm}$-p and $p^{\pm}$-p respectively. These values are close to the limit

$$\frac{\sigma_{el}}{\sigma_T} = \frac{\sigma_T}{16\pi b} \tag{20}$$

and thus satisfy the MacDowell-Martin[50] bound

$$\frac{\sigma_{el}}{\sigma_T} > \frac{\sigma_T}{18\pi b} \tag{21}$$

3.2.3 Structure in Angular Distributions

The experiment of Akerlof et al.[49] provides data for $|t|$ up to $\simeq 3$ GeV^2 for p-p scattering at 100 and 200 GeV/c. These data are very relevant for the discussion of the structure found in p-p scattering at the ISR by Böhm et al.[51] and also reported by Nagy et al.[52] New ISR results by Nagy et al.[53] are presented in Fig. 26 which collects together their data at the equivalent of 290 and 2100 GeV/c, together with that of Akerlof et al. at 100 and 200 GeV/c and of Allaby et al.[54] at 24 GeV/c. The development of the diffraction-like dip and secondary peak begins to be interestingly mapped out. While there is no dip at 100 GeV/c it appears to have developed, although the data are clearly rather tentative, at 200 GeV/c. At ISR energies (290 - 2100 GeV) there is a clear shift towards lower $|t|$. This is also illustrated in Fig. 27 which collects and compares the data on an absolute scale together with results down to 3 GeV/c. Apart from the shift of the diffraction dip the new data also indicate a growth with energy of the secondary diffraction peak. The ISR data have been fitted, Fig. 28, according to a suggestion of Barger and Phillips[55], by a form

$$\frac{d\sigma}{dt} = \left|\sqrt{A}e^{Bt/2} + \sqrt{C}e^{Dt/2+i\phi}\right|^2 \tag{22}$$

This relation fits well in the range $0.6 < |t| < 3.60$ GeV^2 and gives a good estimate of the position of the dip. The latter is given in table 4 together with other relevant data, comprising the slope parameter b, evaluated for $|t|$ between 0.2 and 0.8 GeV, the value of the differential cross section at the secondary maximum and the total cross section.

The information contained in table 4 is consistent with the idea of geometrical scaling[56] (GS) which was implicit in the discussion of the earlier ISR data by Amaldi[1] at Aix-en-Provence. GS means a special behaviour of the scattering amplitude

$$F(s,b) = F\left(a/R(s)\right) \tag{23}$$

where a is the impact parameter and R(s) a radial scale parameter containing all the energy dependence. Then

$$\begin{aligned} \frac{d\sigma}{dt} &= R^4 f(R^2 t) \\ \sigma_T &\sim R^2 \\ b &\sim R^2 \\ t_0 &\sim R^{-2} \end{aligned} \qquad (24)$$

where t_0 is the position of any dip or maximum in $d\sigma/dt$. The data in table 4 are consistent with these relations which simply indicate the consequences of an increasing proton size.

Table 4

Fit parameters for ISR p-p data [53]

	b $[GeV^{-2}]$ $0.2 < \|t\| < 0.8$	$-t_{min}$ $[GeV^2]$	$\frac{d\sigma}{dt}(2^{nd}_{max})$ $[mb/GeV^2]$	σ_{tot} [mb]
$\sqrt{s}$ = 62 GeV	11.2 ± 0.2	1.26 ± 0.03	$(7.2 \pm 1.0) \times 10^{-5}$	44.1 ± 0.9
$\sqrt{s}$ = 23 GeV	9.9 ± 0.2	1.44 ± 0.02	$(4.5 \pm 0.5) \times 10^{-5}$	38.7 ± 0.7
Ratio	1.13 ± 0.3	$(1.14 \pm 0.03)^{-1}$	$(1.27 \pm 0.11)^2$	1.14 ± 0.03
Scaling prediction	$\propto R^2$	$\propto R^{-2}$	$\propto R^4$	$\propto R^2$

The transformation of the p-p scattering amplitude, as far as we know it, into impact parameter space gives, via the overlap functions so obtained, a picturesque impression of the way in which the proton profile changes with energy. A contribution of Grein et al.[57], taking into account real scattering amplitude effects gives the overlap functions at 20 and 1480 GeV shown in Fig. 29. It is claimed that the inelastic overlap function scales geometrically above 50 GeV.

Considering the general way in which the structure develops in Figs. 26 and 27 it is interesting to note that it appears as the real part of the forward scattering amplitude becomes very small (Fig. 19). A possibility is that the diffractive structure is obscured by real part or dispersive effects which so decrease with energy that the structure emerges between 100 and 200 GeV. Spin dependent effects, which, as will be seen in a later section, are not small at large $|t|$, may also play a part.

What about similar structure, that is increasing with energy rather than decreasing Regge-wise, in other hadronic scattering systems? A good candidate would be K^+-p

scattering which shares with p-p the property of having no s-channel resonances. Fig. 30 shows data of Akerlof et al.[49] on K^+-p scattering at 100 GeV/c over a cross section decrease of more than four decades for a $|t|$ range of about 2 GeV . The data appear to fall on a rather smooth curve. Fig. 31 presents π^--p results at 200 GeV/c from the same group. There is the hint of a change of slope at $|t| \simeq 0.4$ GeV^2.

At lower energies the Karlsruhe-ITEP group[58] have measured n-p scattering for momentum transfers up to $|t| \simeq 2.5$ GeV^2. Fig. 32 shows the results together with the trend of p-p elastic scattering at 24 GeV/c[54]. The n-p data exhibit a kink in the distributions at around $|t| \simeq 1.3$ GeV^2, qualitatively similar to that exhibited by the p-p results although less pronounced. This is somewhat at variance with a comparison made by Amaldi et al[59], of 24 GeV/c p-n data obtained from p-d scattering with the 24 GeV/c p-p results of Allaby et al.[54]. In the latter the p-n and p-p angular distributions were identical. The extension of n-p or p-n data to much higher energies will be interesting in the light of the development of the p-p diffractive structure.

3.3 Backward Scattering

Backward scattering data of π^-p are presented by Babaev et al.[60] for momenta of 24.7 and 37.8 GeV/c. The backward peaks shown in Fig. 33 indicate, as at lower energies Δ exchange. The cross sections for the process are big enough to give confidence in the feasibility of backward scattering measurements at considerably higher energies, the differential cross section at $|u| = 0$ varying as $\sim p^{-2.2}$.

3.4 Hyperon Scattering

Bubble chamber results on Λ-p elastic scattering, by a Cambridge University Group[61], are shown in Fig. 34. In a momentum bin of 8 to 24 GeV/c the Λ-p total elastic cross section is 6.0 ± 1.5 mb and the slope parameter b = 10 ± 2 GeV^{-2}. Taking the total cross section data of Gjesdal et al.[62], σ_T (6-21 GeV/c) = 34.6±0.4 mb, one finds that $\sigma_{el}/\sigma_T = 0.17 \pm 0.04$. Clearly studies of hyperon-nucleon scattering and total cross section will become of more and more interest as high energy hyperon beams are developed at the big accelerators. Measuring cross sections at relatively low energies will remain, however, a hard problem.

3.5 Spin Dependence in Elastic Scattering

A summary of recent data on spin dependence in elastic hadron scattering is given in table 5.

The study of the spin dependence of scattering cross sections provides constraints on the possible dynamical situation via the phenomenology, Regge, or optical, presently available. Thus studies of polarization phenomena have been pursued over a wide range up to 45 GeV/c during the past two years.

A survey of the polarisation parameter P in p-p scattering is given in Fig. 35 for momenta between 5 and 45 GeV/c. The picture at 12 GeV/c involving two double zeroes and two maxima changes drastically as the momentum increases to 45 GeV/c. The structure at 12 GeV/c is well described (Fig. 36) by the Indiana group, Bryant et al.[63], in terms of

Table 5

Group	Particles	Momentum Range (Gev/c)	$\|t\|$ Range (GeV^2)	Spin dependent parameter
Indiana	p	12.3 3 and 6	1-6 0.3-1.7	P D
Saclay, IHEP, Dubna, Moscow	π^-, K^-, $\bar{p}$ π^+, K^+, p π^-, K^- π^+ p	40 45 40 45 45	0.08-1.2 0.2-0.5	P P R R R↔C
Michigan, ANL, St. Louis	polarised p	2-6		$\sigma_{T\uparrow\downarrow}-\sigma_{T\uparrow\uparrow}$
ANL	polarised p on deuterium	2-6	0.2-1.0	(pp) P (pn) P

an optical model of Chu and Hendry[64]. At 45 GeV/c the rapid change of P is supposed, by the French-Soviet collaboration, Gaidot et al.[65], to result from the interference of spin flip and non flip amplitudes of the Pomeron resulting in strong negative polarisation. The interest of this result, and its pursuit to higher energies, with regard to the structure in the p-p elastic angular distribution at high energies is clear.

That polarization effects may not necessarily be very small at high energies is demonstrated by Fig. 37 showing $\bar{p}$-p polarization data of Gaidot et al.[65] at 40 GeV/c. Comparison with other data is difficult as there is virtually none. Fig. 37 indicates a strong variation of the real part of the flip amplitude with a zero at $|t| \simeq 0.5$ GeV^2.

Bryant et al.[63] present data on the Wolfenstein depolarization parameter[66] D in p-p scattering at 3 and 6 GeV/c over the $|t|$ range from 0.3 to 1.7 GeV . This parameter, which can be used to place constraints on the scattering amplitude, is given by

$$D = \frac{(1+PP_t)\ P_r - P}{P_t} \qquad (25)$$

where P_r is the recoil proton polarization resulting from the elastic scatter of an unpolarized proton from a polarized target of polarization P_t and P is the elastic p-p polarization parameter. Fig. 38 shows the results together with a fit of the model used to describe the polarization. One may note that for $|t| < 1$ GeV^2 D is almost unity, that is the spin of the target proton is not violently changed in the collision.

A study of the spin rotation parameter R has been made by the French-Soviet collaboration, Pierrard et al.[67]. The experiment involves protons polarized in the scattering plane perpendicular to the beam direction and analysis of the azimuthal distribution of recoil scatterings on carbon. Fig. 39 shows the R distribution for the π^- data at 40 GeV/c.

At 45 GeV/c the average R value for $\pi^+ p$ is found to be -0.22 ± 0.16. The curves drawn in Fig. 39 are the predictions of a Regge pole model[68] with Reggeon-Reggeon cut and of a Regge pole fit[69] containing continuous momentum sum rules.

Pierrard et al.[67] have also performed measurements on p-p scattering at 45 GeV/c to determine the linear combination

$$C = R\sin\alpha - |A|\cos\alpha \qquad (26)$$

involving the spin parameter A and α, an angle equal to 90° at 45 GeV/c and close to 90° at lower energies. Fig. 40 shows a compilation of C distributions for momenta between 3.8 and 45 GeV/c indicating no significant variation of C with energy.

A comparison of the R and C spin parameters for π-p and p-p scattering suggests that they are very similar. A possible simple explanation[67] is that of Pomeron dominance and factorisation.

An amplitude analysis has been performed[67] on the π-p data at 40 GeV/c. The isospin zero helicity amplitudes determined were found to exhibit $|t|$ dependences very similar to those at 6 and 16 GeV/c. Fig. 41 shows, essentially, the ratio of flip to non flip amplitudes as a function of momentum, there is evidently no strong energy dependence.

The introduction of a high energy polarised proton beam has provided new possibilities at ANL. Experiments[70] using the polarized beam to scatter on polarized hydrogen have measured the total cross sections for the two spins aligned and opposed. Fig. 42 shows the results obtained up to 6 GeV/c, a very rapid fall off being manifested in the difference between the two cross sections. The cross section differences are 5.75 ± 0.69 mb and 0.25 ± 0.05 mb at 2 and 6 GeV/c respectively. A zero cross section difference would be expected[71] for factorising exchange models.

Diebold et al.[72] have studied the polarisation parameter for p-p and p-n scattering using the polarised proton beam and a deuterium target. Their data between 2 and 6 GeV/c are shown in Fig. 43 and may be used to separate the isospin 0 and 1 t channel exchange contributions to the spin flip amplitude. Pure isoscalar exchange would produce equal polarisations for p-p and p-n scattering while pure isovector exchange would give mirror symmetry $P(pn) = -P(pp)$ as for $\pi^\pm$-p scattering. As the data indicate neither equality nor mirror symmetry, both isoscalar and isovector exchanges are needed in the single flip amplitudes.

4. CONCLUDING REMARKS

A brief summary of the main points of this report may be made as follows.

(i) A convenient description of the energy dependence of hadronic total cross sections may be provided in terms of two components. A decreasing component is adequately furnished by Regge phenomenology while the rising component remains ill defined. The functional forms of the rising cross sections are not yet well determined experimentally, information at yet higher energies being needed.

(ii) The deviations of the behaviour of cross sections from Regge exchange degeneracy and universality and from simple additive quark behaviour are becoming quite well determined up to high energies. A complete and reliable picture involving neutron targets is not available, however, as the procedure used to obtain neutron cross sections appears to be inadequate. Further work, both experimental and theoretical, is needed in this domain.

(iii) The usefulness of the well known connections between the real parts of the forward scattering amplitudes and the total cross sections has been underlined by the latest results. The necessity for real part data up to the very highest energies, to provide at least a consistent picture with total cross sections, is evident.

(iv) Geometrical scaling, in its simplest form, provides a very useful picture in scattering processes and should provide a valuable constraint in discussing the various particle systems.

(v) Backward elastic scattering appears to be experimentally feasible up to rather high energies and the resulting data will be invaluable in providing information on Regge exchange processes.

(vi) The study of spin dependence in scattering processes appears to be feasible to higher energies than once foreseen, first because the spin effects are not too small and secondly because experimental techniques are increasingly sensitive. The results on the various spin parameters begin to open up the possibility of amplitude analyses and should provide possibilities for distinguishing between various phenomenological schemes.

References

1) U. Amaldi, Proc. II International Conf. on Elementary Particles, (Aix--en- Provence) Journal de Physique, Tome 34, C1 - 1973, p.241.

2) G.C. Beznogikh et al., Phys. Lett. 30B (1969), 274.
G.C. Beznogikh et al., Phys. Lett. 39B (1972), 411.

3) S.P. Denisov et al., Phys. Lett. 36B (1971), 415.

4) A.S. Carroll et al., Phys. Rev. Lett. 33 (1974), 928, and 33 (1974), 932.

5) C. Baglin et al., to be published in Nuclear Physics.

6) A.N. Diddens, Proc. XVII Int. Conf. on High Energy Physics, London (1974), p. I-41.

7) K. Eggert et al., conference contribution G1-38.

8) S.R. Amendolia et al., Phys. Lett. 44B (1973), 113.

9) U. Amaldi et al., Phys. Lett. 44B (1973), 112.

10) A.S. Carroll et al., conference contribution G1-01, to be published in Phys. Lett.

11) R.J. Glauber, Phys. Rev. 100 (1955), 242.
C. Wilkin, Phys. Rev. Lett. 17 (1966), 561.

12) M.J. Longo et al., Phys. Rev. Lett. 33 (1974), 725.

13) S.P. Denisov et al., Phys. Lett. 36B (1971), 528 and Nucl. Phys. B56 (1973), 1.

14) L.B. Okun and I.Ya. Pomeranchuk, JETP 3 (1958), 307.

15) E. Leader et al., submitted to Nuovo Cimento.

16) A.V. Barnes et al., Proc. XVII, Int. Conf. on High Energy Physics, London (1974), p. I-37.

17) R.E. Hendrick et al., Phys. Rev. 11D (1975), 536.

18) E.M. Levin and L.L. Frankfurt, JETP Lett. 2 (1965), 65.

19) K. Johnson and S.B. Treiman, Phys. Rev. Lett. 14 (1965), 189.

20) D.R.O. Morrison, Proc. Roy. Soc. A335 (1973), 461.

21) K. Goulianos, conference contribution G1-36.

22) M. Froissart, Phys. Rev. 123 (1961), 1053.

23) W. Bartel and A.N. Diddens, CERN Internal Report NP 73-4 (1973) and reference 6.

24) H.J. Lipkin, priv. comm. at conference.

25) H.J. Lipkin, Phys. Lett. 56B (1975), 76.

26) G. Giacomelli, Proc. XVI Int. Conf. on High Energy Physics, Chicago-Batavia, Vol. 3, p. 219.

27) V. Barger and R.J.N. Phillips, preprint Univ. of Wisconsin COO-881-445 (1975).

28) U. Camerini et al. contribution to conference.
B. Knapp et al., Phys. Rev. Lett. 34 (1975), 1040.
G. Theodosiu et al., contribution to conference.

29) C.C. Ting, session A-1 of conference.

30) V. Barger and R.J.N. Phillips, Univ. of Wisconsin, preprint COO-462 (1975).

31) N.N. Khuri and T. Kinoshita, Phys. Rev. 137B (1965), 720 and 140B (1965), 706.

32) J.B. Bronzan, ANL/HEP 7327 (1973), p.33.
N.N. Gribov and A.A. Migdal, Sov. J. Nucl. Phys. 8 (1969), 702.
J.B. Bronzan, G.L. Kane and U.P. Sukhatme, Phys. Lett. 49B (1974), 272.

33) D.R. Sidhu and U.P. Sukhatme, Phys. Rev. 11D (1975), 1351.

34) R.E. Hendrick and B. Lautrup, Phys. Rev. 11D (1975), 529.

35) V. Bartenev et al., Phys. Rev. Lett. 31 (1973), 1367.

36) U. Amaldi et al., Phys. Lett. 43B (1973), 231.

37) FNAL - Yale Group, J. Lach, priv. comm.

38) P. Jenni et al., to be published in Nucl. Phys. B.

39) P. Baillon et al., Phys. Lett. 50B (1974), 387.

40) K.J. Foley et al., Phys. Rev. 181 (1969), 1755.

41) V.D. Apokin et al., Phys. Lett. 56B (1975), 391.

42) P. Baillon et al., Phys. Lett. 50B (1974), 377.

43) T.H.H. Bellm et al., Phys. Lett. 33B (1970), 438.
J.R. Campbell et al., Nucl. Phys. B64 (1973), 1.
Amsterdam-Nijmegen-Ecole Polytechnique Collaboration, submitted to Second International Conference on Elementary Particles, Aix-en-Provence 1973 (unpublished).

44) J. Kluyver and R. Salmeron, priv. comm.

45) CERN-Rome collaboration, CERN/ISRC/74-17 (1974).

46) Single Arm Spectrometer Group, contribution to conference and Fermilab-Pub-75/48-EXP (submitted to Phys. Rev. Letts.).

47) Yu.M. Antipov et al., contribution to conference.

48) G. Barbiellini et al., Phys. Letts. (1972), 663.

49) Michigan, ANL, FNAL, Indiana collaboration. D. Jovanovic, priv. comm.

50) S.W. MacDowell and A. Martin, Phys. Rev. 135B (1964), 960.

51) A. Böhm et al., Phys. Lett. 49B (1974), 491.

52) E. Nagy et al., Proc. 17th International Conference on High Energy Physics, London (1974), p. I-30.

53) E. Nagy et al., conference contribution G1-29, submitted to Phys. Lett.

54) J.V. Allaby et al., Nucl. Phys. B52 (1973), 316.

55) R.J.N. Phillips and V. Barger, Phys. Lett. 46B (1973), 412.

56) J. Dias de Deus, Nucl. Phys. B59 (1973), 231.
A.J. Buras and J. Dias de Deus, Nucl. Phys. B71 (1974), 481.

57) W. Grein et al., conference contribution G1-24.

58) V. Böhmer et al., conference contribution G1-37 and submitted to Nucl. Phys.

59) U. Amaldi et al., Nucl. Phys. B39 (1972), 39.

60) A. Babaev et al., conference contribution G2-13.

61) R.P. Mount et al., conference contribution G1-11.

62) S. Gjesdal et al., Phys. Lett. 40B (1972), 152.

63) G.W. Bryant et al., conference contribution G1-27.

64) S.Y. Chu and A.W. Hendry, Phys. Rev. D6 (1972), 190 and T.Y. Cheng et al. Phys. Rev. D7 (1973), 86.

65) A. Gaidot et al., contribution to the conference and Phys. Lett. 57B (1975), 389.

66) L. Wolfenstein, Phys. Rev. 96 (1954), 1654.

67) J. Pierrard et al., contribution to the conference and Phys. Lett. 57B (1975), 393.

68) G. Girardi et al., Nucl. Phys. B47 (1972), 445.

69) V. Barger and R.J.N. Phillips, Phys. Rev. 187 (1969), 2210.

70) W. de Boer et al., Phys. Rev. Lett. 34 (1975), 558.

71) E. Leader, Rev. Mod. Phys. 38 (1966), 476.

72) R. Diebold et al., submitted to Phys. Rev. Lett.

Figure Captions

Fig. 1 Rising K^+-p total cross section, London Conference 1974. The curve is a fit described in Ref. 17

Fig. 2 p-p total cross sections at the time of the London Conference 1974. The curve is a fit described in Ref. 17.

Fig. 3 Elastic scattering angular distributions for various hadronic systems (Ref. 5).

Fig. 4 Compilation of hadron-proton total cross sections including new measurements (Ref. 10).

Fig. 5 Compilation of hadron-deuteron total cross sections including new data (Ref. 10).

Fig. 6 Deuteron radius parameter $\langle r^{-2} \rangle$ obtained from high energy pion cross sections (Ref. 10).

Fig. 7 Compilation of hadron-neutron total cross sections including new data (Ref. 10).

Fig. 8 Particle-antiparticle cross section differences. The lines shown are power law fits (Ref. 10).

Fig. 9 p-p and $\bar{p}$-p cross sections. The broken line indicates an extrapolation of the $\bar{p}$-p cross section using the p-p trend and the power law difference given in Fig. 8 (Ref. 10).

Fig. 10 Present status of evidence for ω and for ρ-ω universality over a momentum range up to 200 GeV/c. (Priv. comm. W.F. Baker).

Fig. 11 Present status of evidence for A_2 universality (priv. comm. W.F. Baker).

Fig. 12 Status of simple additive quark model ratios for momenta up to 200 and 240 GeV/c (priv. comm. K.P. Pretzl).

Fig. 13 Test of first Johnson-Treiman relation for momenta up to 240 GeV/c (priv. comm. W.F. Baker).

Fig. 14 Test of second Johnson-Treiman relation for momenta up to 240 GeV/c (priv. comm. W.F. Baker).

Fig. 15 Lipkin plot (Ref. 24) of hadronic total cross sections.

Fig. 16 Compilation of photon-proton total cross sections (Ref. 26).

Fig. 17 Total cross sections for ρ^0-p and ϕ-p obtained by vector dominance model considerations from photoproduction data (Ref. 27).

Fig. 18 ψ-p total cross sections obtained (Ref. 30) from photoproduction data (Ref. 28).

Fig. 19 Momentum dependence of ρ for p-p scattering. Recent data Refs. 35, 36 and 37. The curves indicate the results of a dispersion relation evaluation (Ref. 34).

Fig. 20 Momentum dependence of ρ for $\bar{p}$-p scattering. Recent data, Refs. 37 and 38. The results of a dispersion relation evaluation are indicated (Ref. 34).

Fig. 21 Momentum dependence of ρ for π^+-p scattering (Refs. 37, 39 and 40). The curves show the results of a dispersion relation calculation (Ref. 34).

Fig. 22 ρ as a function of momentum for π^--p scattering. The data at the highest energies are from Refs. 37 and 41. The trend of a dispersion relation evaluation is shown (Ref. 34).

Fig. 23 Momentum dependence of ρ for K^+-p scattering. The point at 70 GeV/c is from Ref. 37. The results of a dispersion relation calculation are shown (Ref. 34).

Fig. 24 ρ as a function of momentum for K^--p scattering, data from Refs. 37, 42, 43 and 44. The curves show the results of a dispersion relation calculation (Ref. 34).

Fig. 25 Compilation of the diffraction peak slope parameter b_e (Ref. 46). New data from Ref. 47 are also shown.

Fig. 26 t distributions for p-p elastic scattering (Refs. 49, 53 and 54). Note displacement of vertical scales.

Fig. 27 Compilation of p-p elastic scattering data. The results at highest energies are from Refs. 49 and 53).

Fig. 28 Fit to ISR p-p scattering data (Ref. 53) using a form suggested in Ref. 55.

Fig. 29 Impact parameter space overlap functions for p-p scattering at 20 GeV (continuous lines) and 1480 GeV (broken lines) (Ref. 57).

Fig. 30 t distribution for K^+-p elastic scattering at 100 GeV/c (Ref. 49).

Fig. 31 t distribution for π^--p elastic scattering at 200 GeV/c (Ref. 49).

Fig. 32 Elastic scattering distributions for n-p collisions (Ref. 58). The curve indicates the result of Ref. 59 for p-p scattering at 24 GeV/c.

Fig. 33 Results on π^--p backward scattering at 24.7 and 37.8 GeV/c (Ref. 60).

Fig. 34 Total elastic cross sections and diffraction peak slope parameters for Λ-p elastic scattering (Ref. 61).

Fig. 35 A compilation of the momentum transfer dependence of the polarisation parameter for p-p elastic scattering between 5 and 45 GeV/c. The data at 45 GeV/c are from Ref. 65.

Fig. 36 Results on the polarisation parameter in p-p elastic scattering at 12.3 GeV/c (Ref. 63). The curve shown is the result of an optical model calculation using the procedure of Ref. 64.

Fig. 37 The t dependence of the polarisation parameter for $\bar{p}$-p elastic scattering at 40 GeV/c (Ref. 65).

Fig. 38 The t dependence of the Wolfenstein depolarisation parameter, D,for p-p scattering at 3 and 6 GeV/c (Ref. 63). The curve indicates the result of a calculation using an optical model described in Ref. 64.

Fig. 39 The momentum transfer dependence of the spin rotation parameter, R, in $\bar{\pi}$-p scattering at 40 GeV/c (Ref. 67). The broken curve indicates a Regge pole fit (Ref. 69), the dash-dot curve a model involving Regge cuts (Ref. 68) and the continuous curve a dependence - $\cos\theta_{\text{proton}}$.

Fig. 40 Data on the p-p scattering spin parameter C at various momenta (Ref. 67).

Fig. 41 Momentum dependence of the ratio of isospin 0 spin flip to non flip amplitudes for π-p scattering (Ref. 67) τ_0 includes a factor $\sqrt{s_0/|t|}$ where $s_0 = 1$ GeV^2 and $|t| = 0.35$ GeV^2. The curve shown is a prediction of the theory of Ref. 69.

Fig. 42 Momentum dependence of the difference between the total cross sections of protons interacting with spins aligned and anti-aligned (Ref. 70).

Fig. 43 Polarisation parameter for p-p and p-n scattering between 2 and 6 GeV/c (Ref. 72).

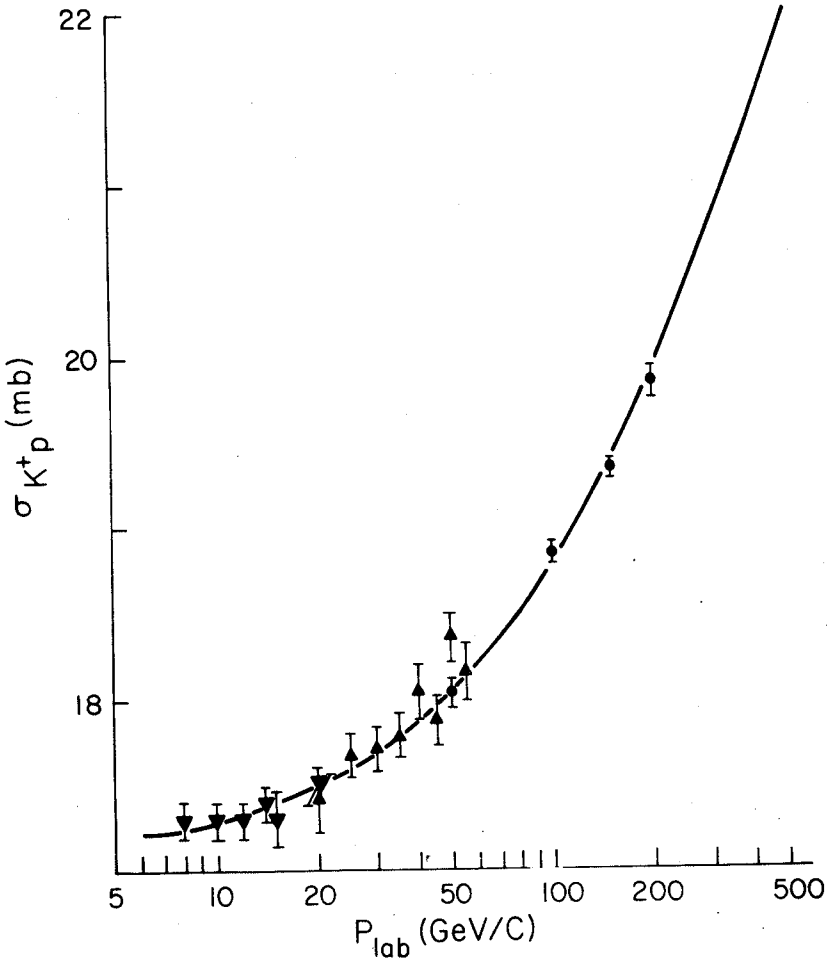
22
20
18
σ_{K^+p} (mb)
5
10
20
50
100
200
500
P_{lab} (GeV/C)

Fig. 1

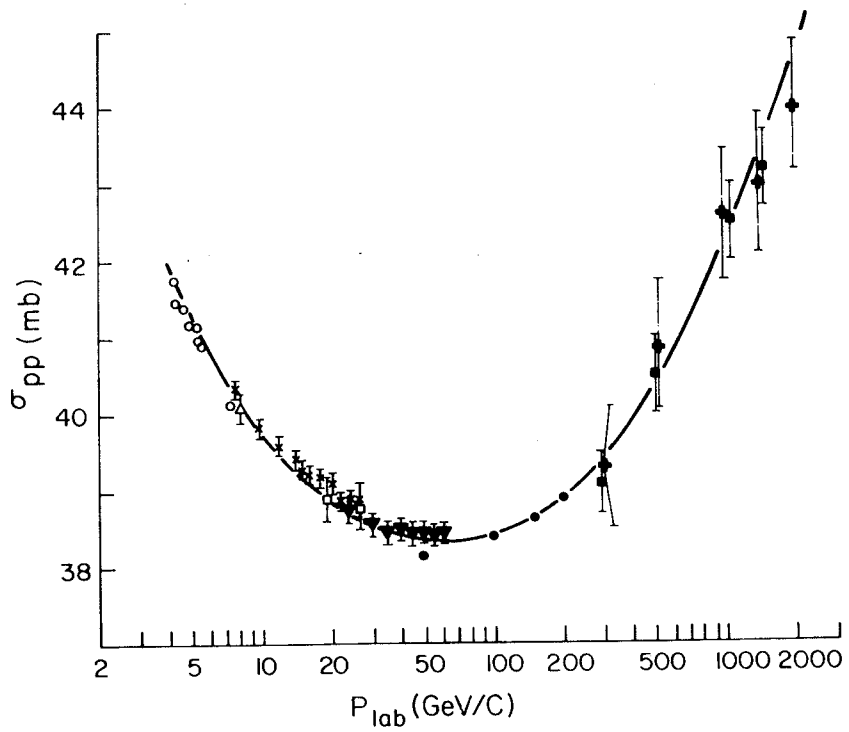
44
42
40
38
σ_{pp} (mb)
2
5
10
20
50
100
200
500
1000
2000
P_{lab} (GeV/C)

Fig. 2

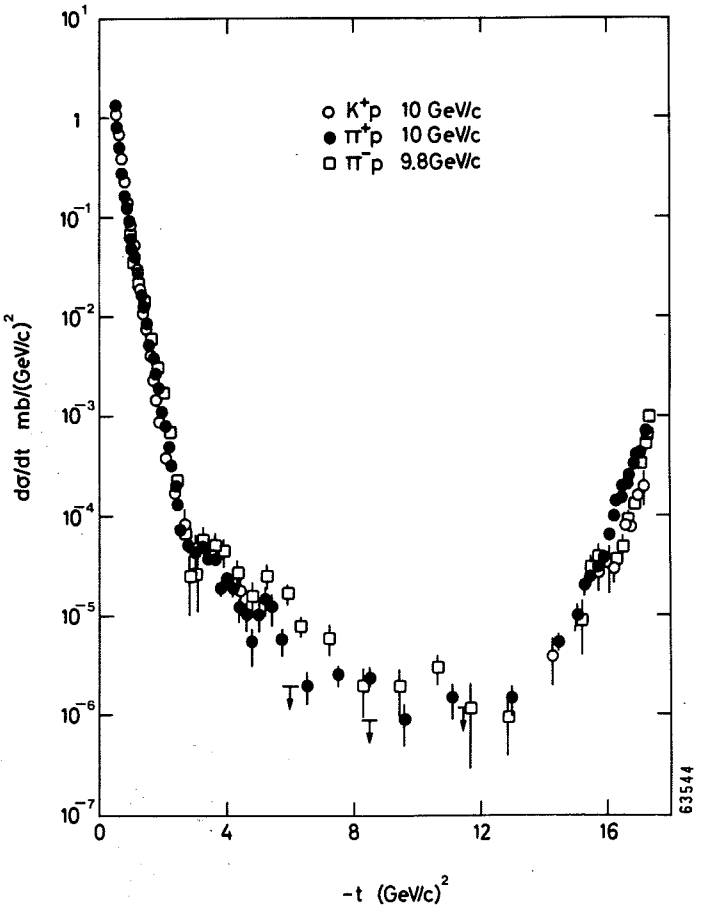
o K+p 10 GeV/c
● π+p 10 GeV/c
□ π−p 9.8GeV/c
dσ/dt mb/(GeV/c)²
-t (GeV/c)²
63544

Fig. 3

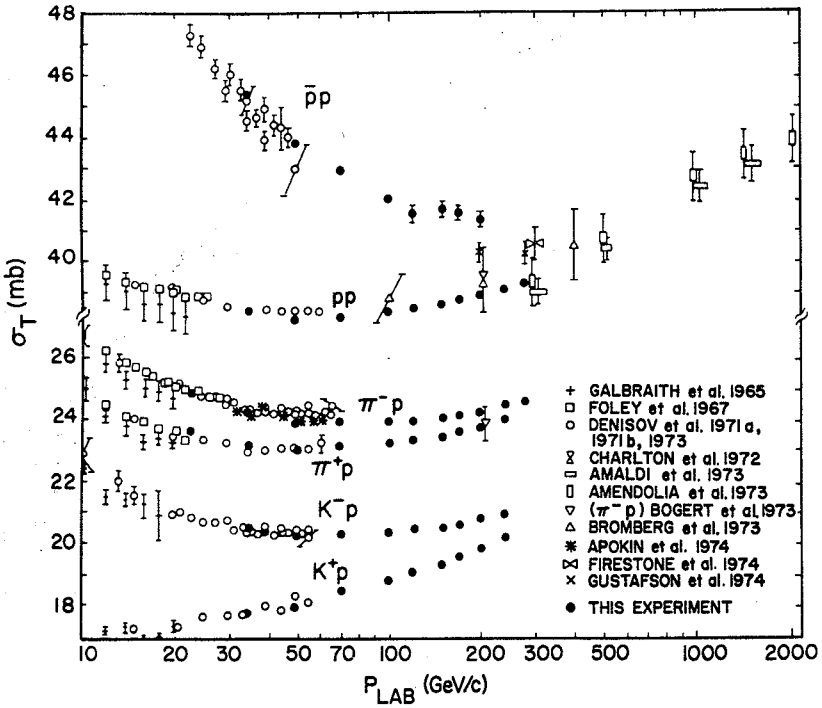
σT (mb)
P_LAB (GeV/c)
p̄p
pp
π⁻p
π⁺p
K⁻p
K⁺p
+ GALBRAITH et al. 1965
□ FOLEY et al. 1967
o DENISOV et al. 1971a, 1971b, 1973
⧖ CHARLTON et al. 1972
▭ AMALDI et al. 1973
▯ AMENDOLIA et al. 1973
▽ (π⁻p) BOGERT et al. 1973
△ BROMBERG et al. 1973
✱ APOKIN et al. 1974
⋈ FIRESTONE et al. 1974
× GUSTAFSON et al. 1974
● THIS EXPERIMENT

Fig. 4

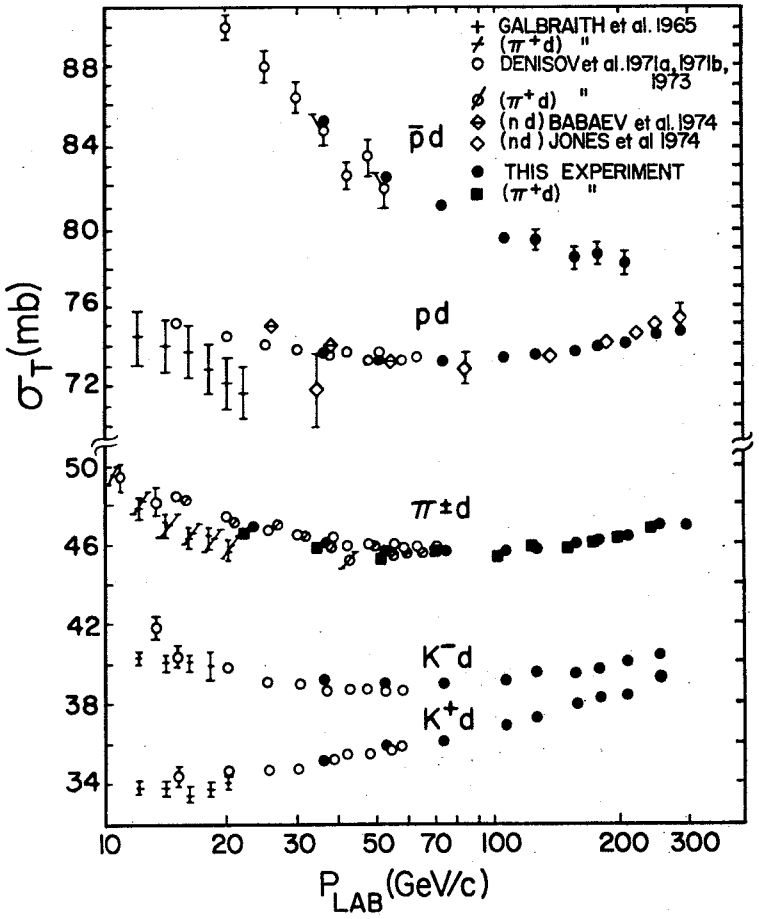
+ GALBRAITH et al. 1965
(π⁺d) "
○ DENISOV et al. 1971a, 1971b, 1973
(π⁺d) "
◇ (n d) BABAEV et al. 1974
◇ (nd) JONES et al 1974
● THIS EXPERIMENT
■ (π⁺d) "
p̄d
pd
π±d
K⁻d
K⁺d
σT(mb)
PLAB(GeV/c)

Fig. 5

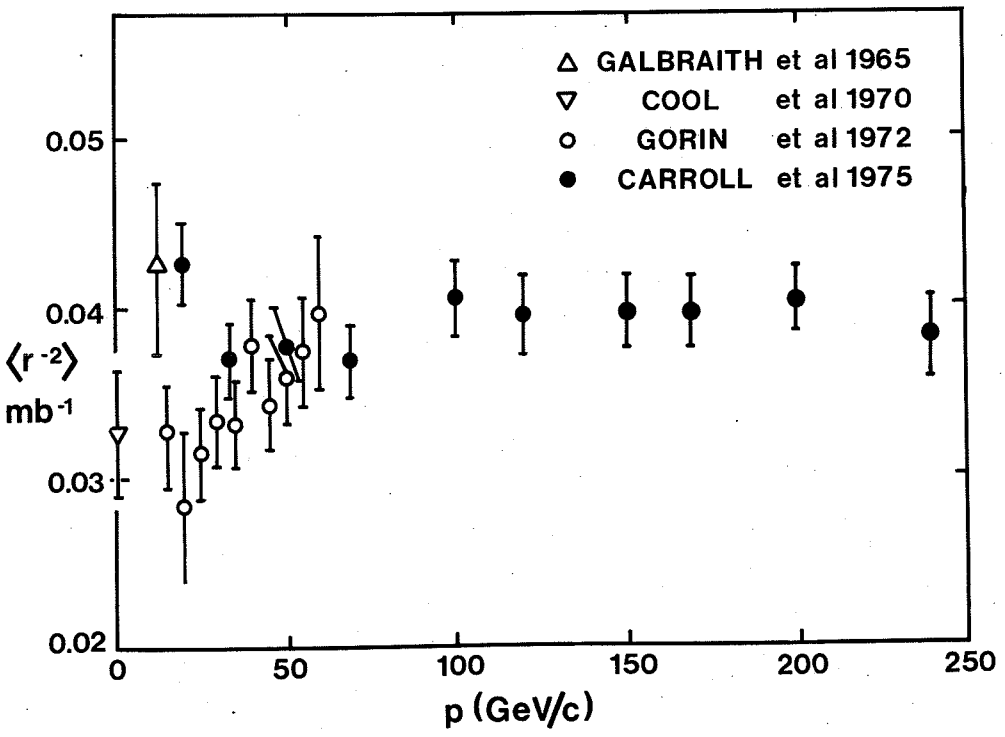
△ GALBRAITH et al 1965
▽ COOL et al 1970
○ GORIN et al 1972
● CARROLL et al 1975
⟨r⁻²⟩
mb⁻¹
p (GeV/c)

Fig. 6

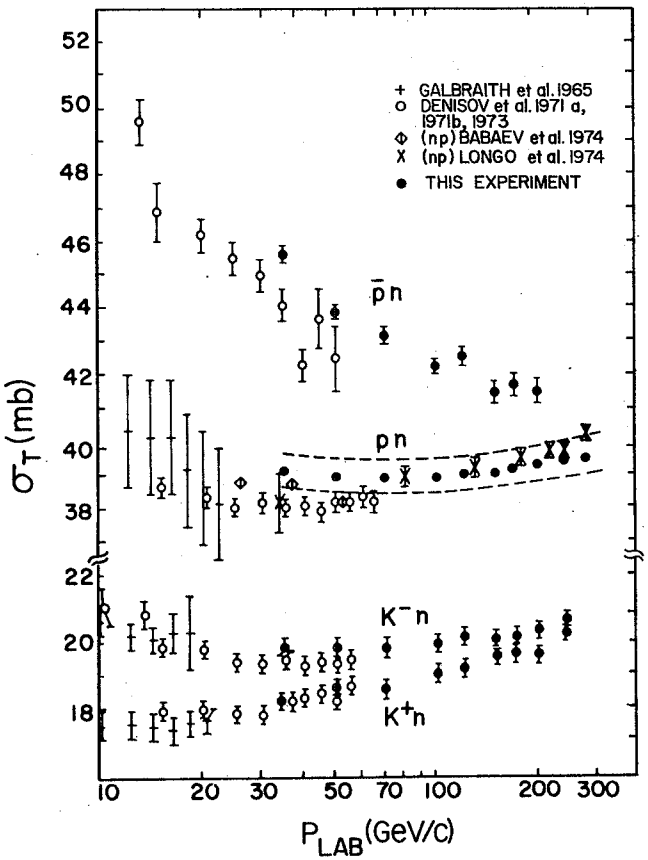
+ GALBRAITH et al. 1965
○ DENISOV et al. 1971 a, 1971b, 1973
Φ (np) BABAEV et al. 1974
X (np) LONGO et al. 1974
● THIS EXPERIMENT
p̄n
pn
K⁻n
K⁺n
σT (mb)
PLAB (GeV/c)

Fig. 7

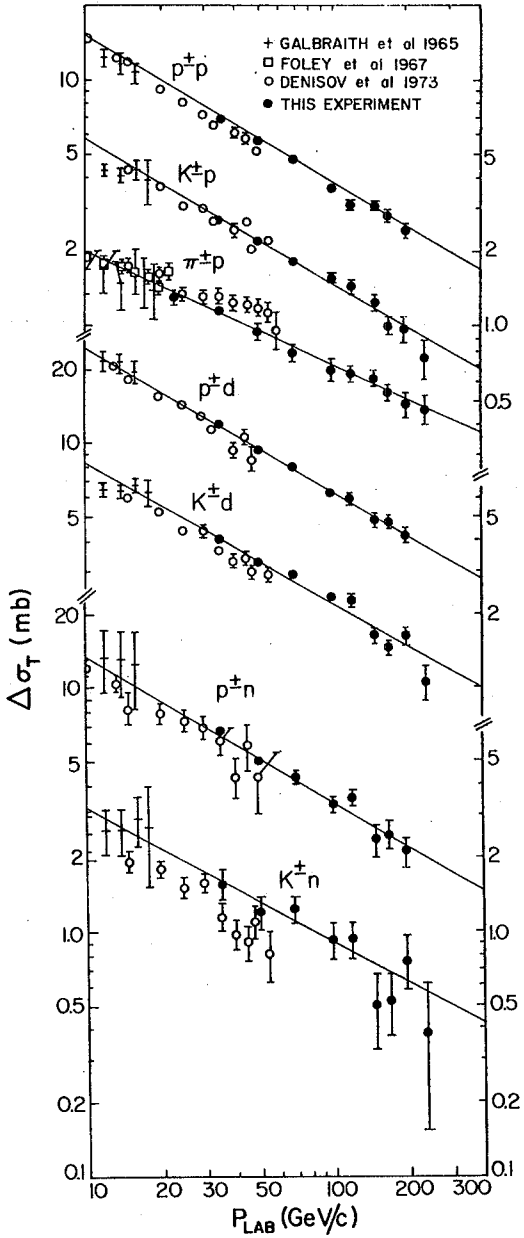
+ GALBRAITH et al 1965
□ FOLEY et al 1967
○ DENISOV et al 1973
● THIS EXPERIMENT
p±p
K±p
π±p
p±d
K±d
p±n
K±n
Δσ T (mb)
PLAB (GeV/c)

Fig. 8

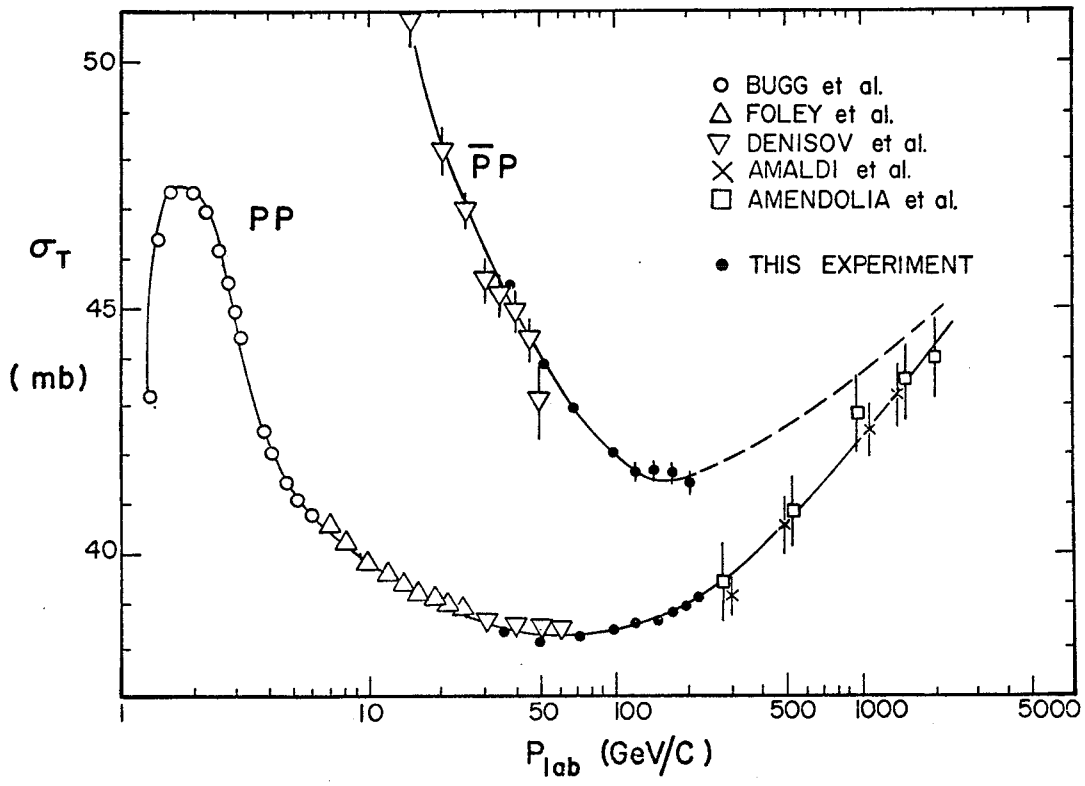
50
45
40
σ_T
(mb)
PP
$\bar{P}P$
BUGG et al.
FOLEY et al.
DENISOV et al.
AMALDI et al.
AMENDOLIA et al.
THIS EXPERIMENT
1
10
50
100
500
1000
5000
P_{lab} (GeV/C)

Fig. 9

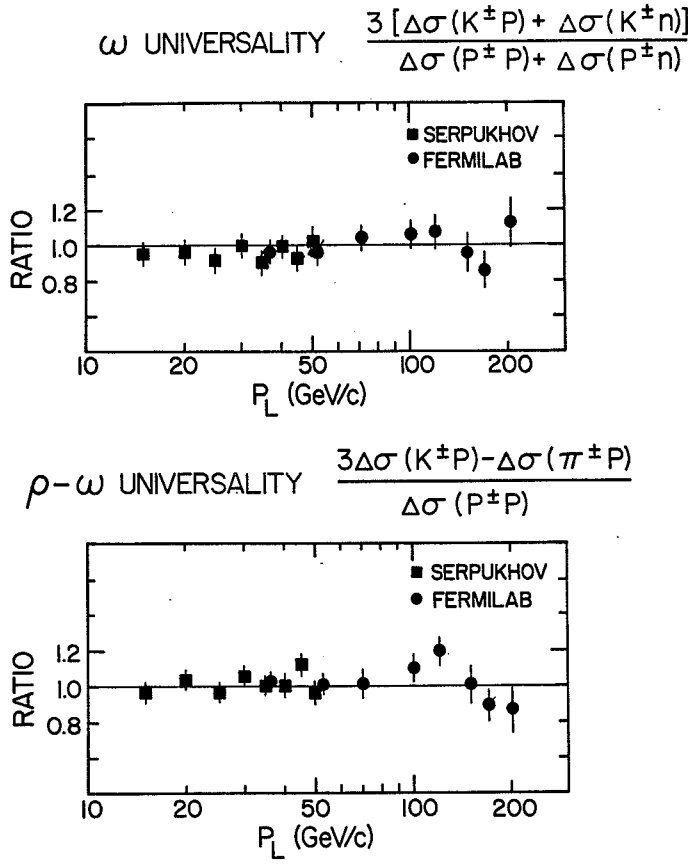
ω UNIVERSALITY
$\frac{3[\Delta\sigma(K^{\pm}P)+\Delta\sigma(K^{\pm}n)]}{\Delta\sigma(P^{\pm}P)+\Delta\sigma(P^{\pm}n)}$
SERPUKHOV
FERMILAB
RATIO
1.2
1.0
0.8
10
20
50
100
200
P_L (GeV/c)
$\rho-\omega$ UNIVERSALITY
$\frac{3\Delta\sigma(K^{\pm}P)-\Delta\sigma(\pi^{\pm}P)}{\Delta\sigma(P^{\pm}P)}$
SERPUKHOV
FERMILAB
RATIO
1.2
1.0
0.8
10
20
50
100
200
P_L (GeV/c)

Fig. 10

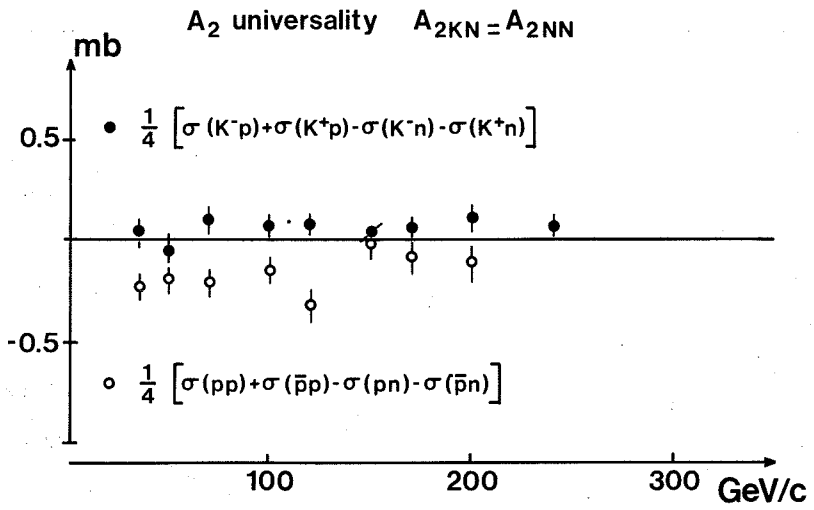
A_2 universality $A_{2KN} = A_{2NN}$
mb
0.5
-0.5
$\frac{1}{4}\left[\sigma(K^-p)+\sigma(K^+p)-\sigma(K^-n)-\sigma(K^+n)\right]$
$\frac{1}{4}\left[\sigma(pp)+\sigma(\bar{p}p)-\sigma(pn)-\sigma(\bar{p}n)\right]$
100
200
300
GeV/c

Fig. 11

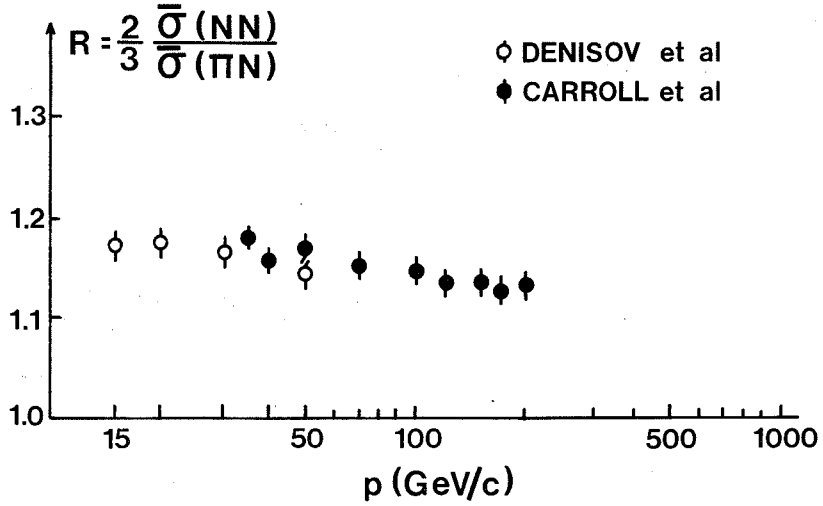
$R = \frac{2}{3}\frac{\bar{\sigma}(NN)}{\bar{\sigma}(\pi N)}$
DENISOV et al
CARROLL et al
1.3
1.2
1.1
1.0
15
50
100
500
1000
p (GeV/c)

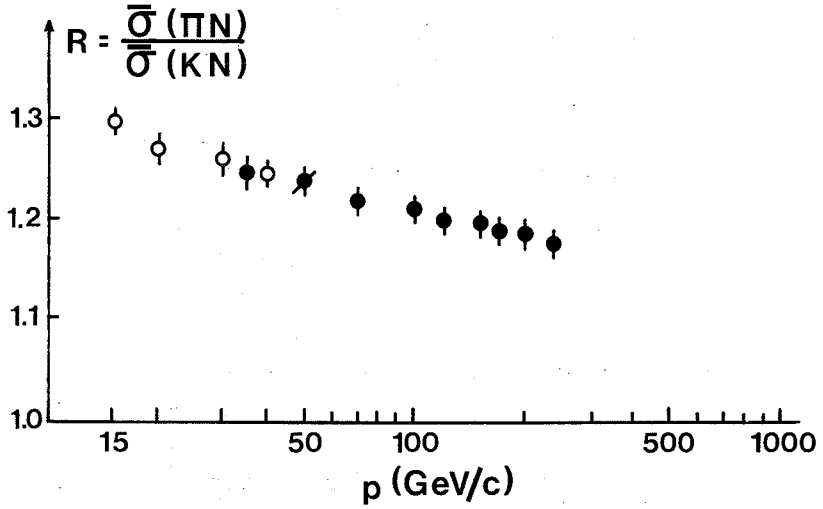
$R = \frac{\bar{\sigma}(\pi N)}{\bar{\sigma}(KN)}$
1.3
1.2
1.1
1.0
15
50
100
500
1000
p (GeV/c)

Fig. 12

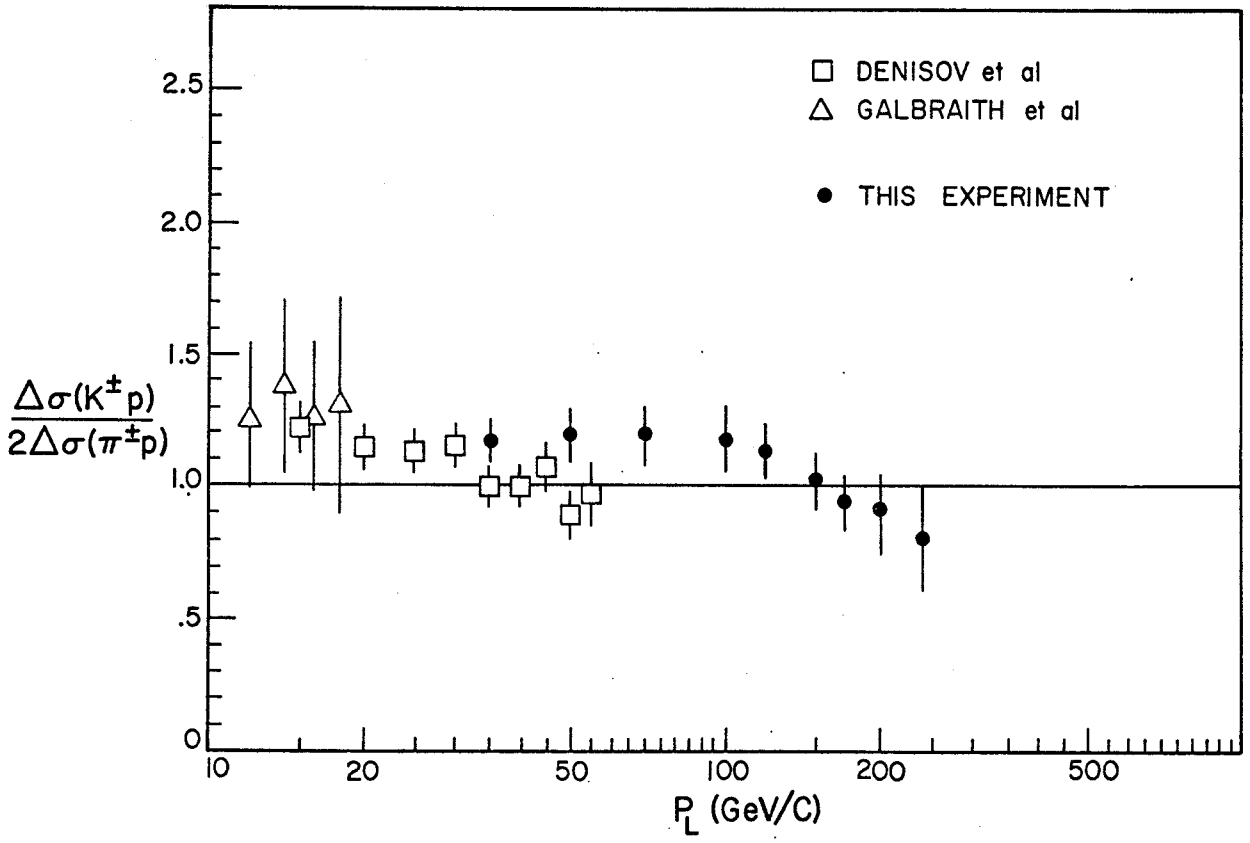
DENISOV et al
GALBRAITH et al
THIS EXPERIMENT
$\frac{\Delta\sigma(K^{\pm}p)}{2\Delta\sigma(\pi^{\pm}p)}$
2.5
2.0
1.5
1.0
.5
0
10
20
50
100
200
500
P_L (GeV/C)

Fig. 13

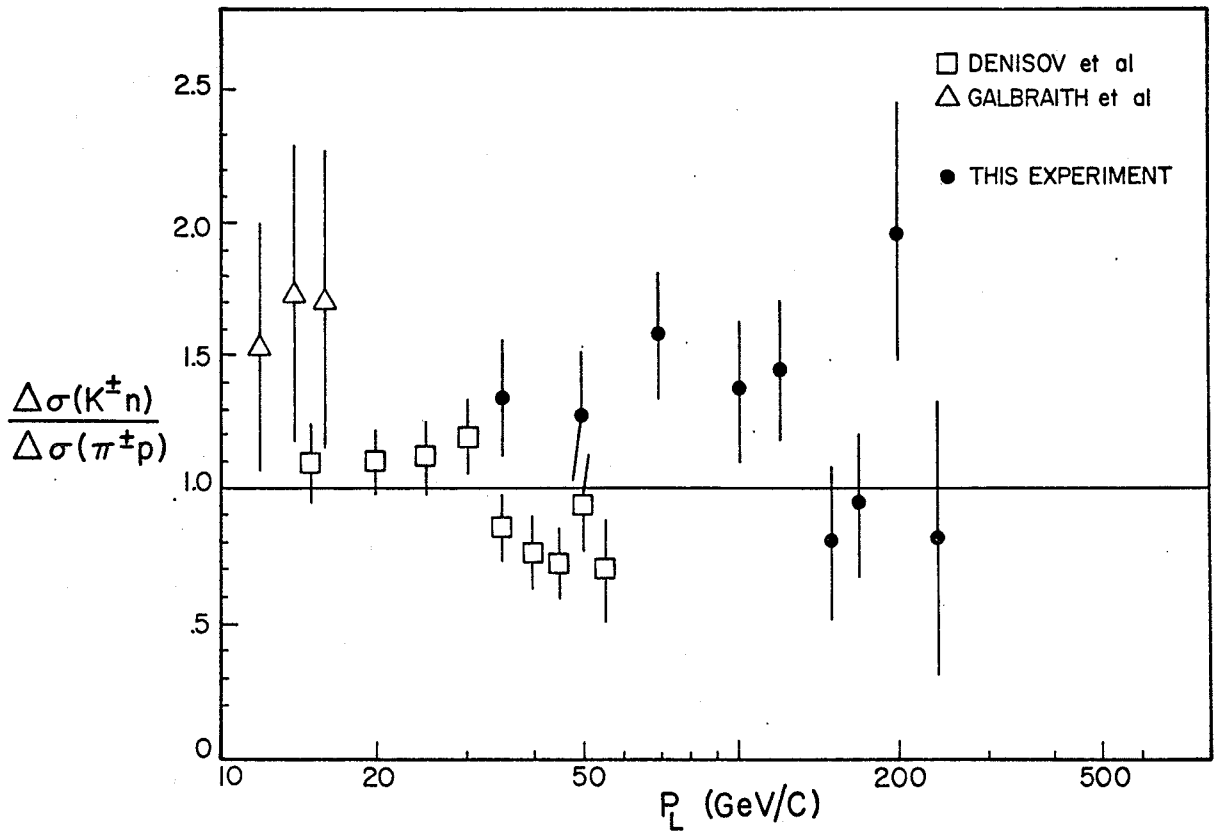
DENISOV et al
GALBRAITH et al
THIS EXPERIMENT
$\frac{\Delta\sigma(K^{\pm}n)}{\Delta\sigma(\pi^{\pm}p)}$
2.5
2.0
1.5
1.0
.5
0
10
20
50
200
500
P_L (GeV/C)

Fig. 14

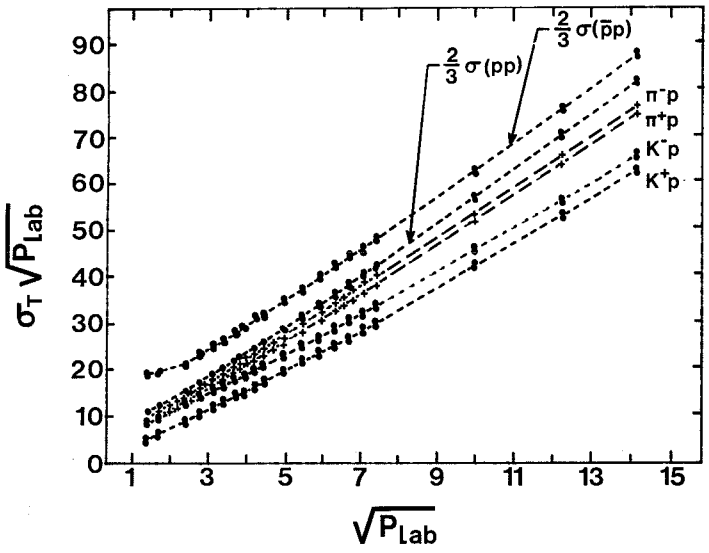
$\frac{2}{3}\sigma(\bar{p}p)$
$\frac{2}{3}\sigma(pp)$
π^-p
π^+p
K^-p
K^+p
$\sigma_T\sqrt{P_{Lab}}$
$\sqrt{P_{Lab}}$

Fig. 15

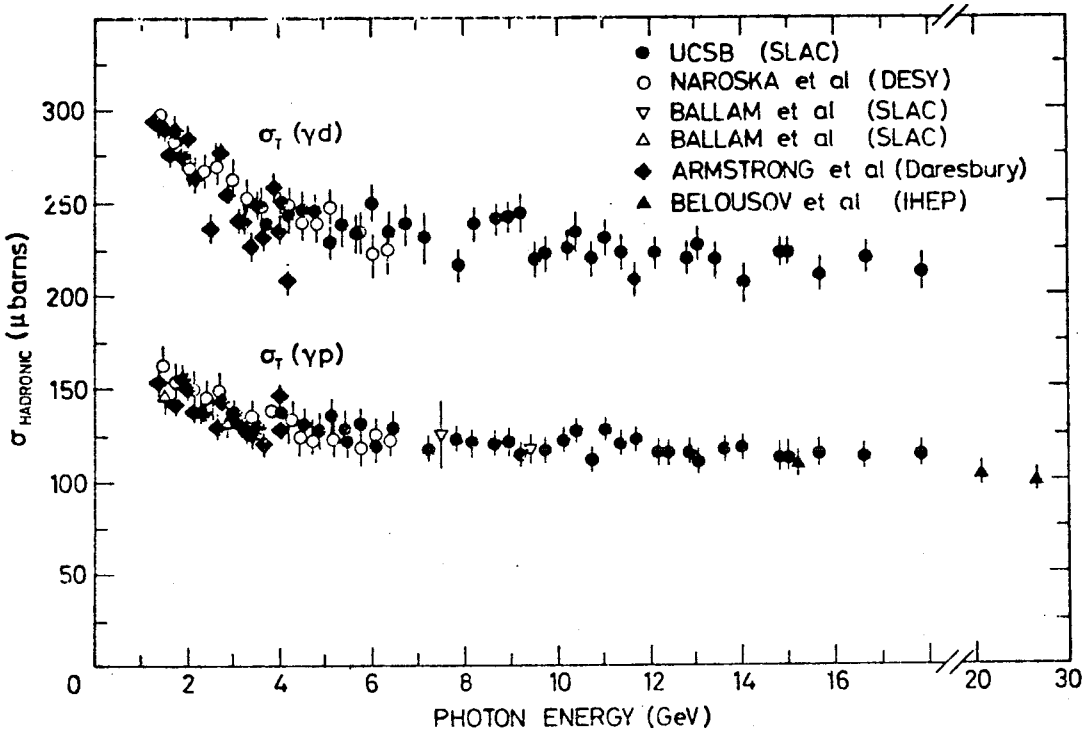
UCSB (SLAC)
NAROSKA et al (DESY)
BALLAM et al (SLAC)
BALLAM et al (SLAC)
ARMSTRONG et al (Daresbury)
BELOUSOV et al (IHEP)
$\sigma_T(\gamma d)$
$\sigma_T(\gamma p)$
$\sigma_{HADRONIC}$ (μbarns)
PHOTON ENERGY (GeV)

Fig. 16

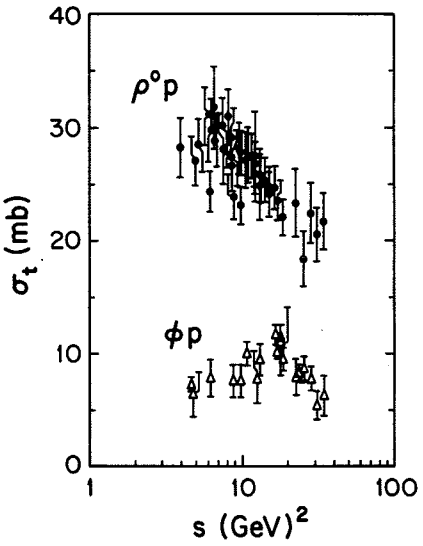
40
30
20
10
0
σ_t (mb)
$\rho^o p$
ϕp
1
10
100
s (GeV)^2

Fig. 17

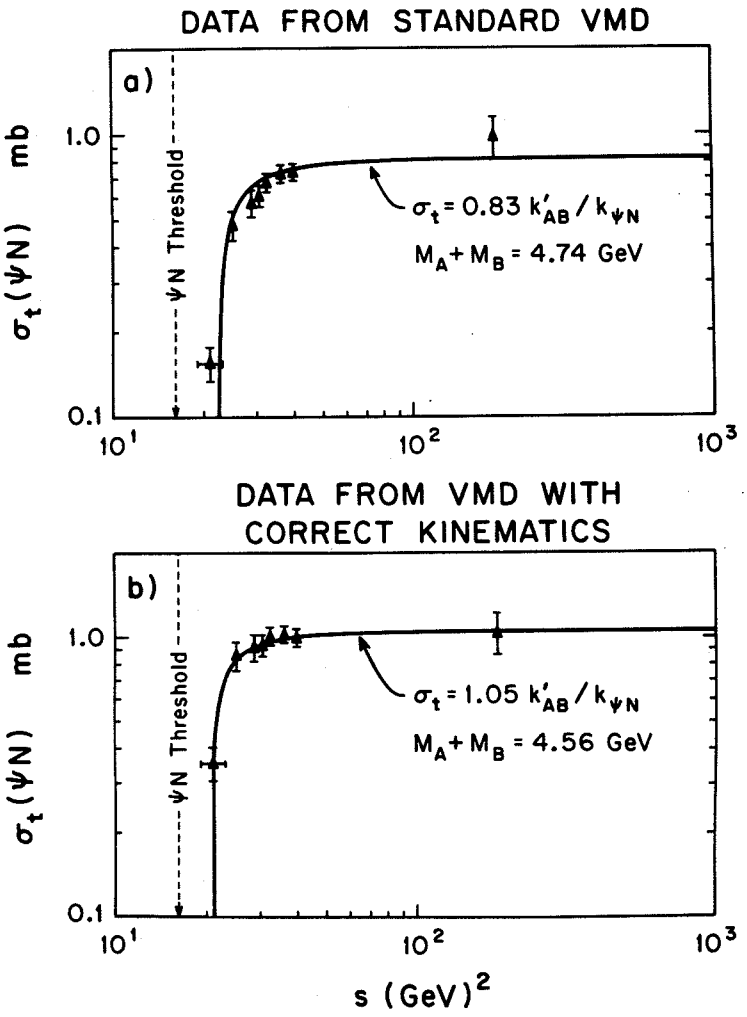
DATA FROM STANDARD VMD
a)
1.0
0.1
$\sigma_t(\psi N)$ mb
ψN Threshold
$\sigma_t = 0.83\ k'_{AB} / k_{\psi N}$
$M_A + M_B = 4.74$ GeV
10^1
10^2
10^3
DATA FROM VMD WITH
CORRECT KINEMATICS
b)
1.0
0.1
$\sigma_t(\psi N)$ mb
ψN Threshold
$\sigma_t = 1.05\ k'_{AB} / k_{\psi N}$
$M_A + M_B = 4.56$ GeV
10^1
10^2
10^3
s (GeV)^2

Fig. 18

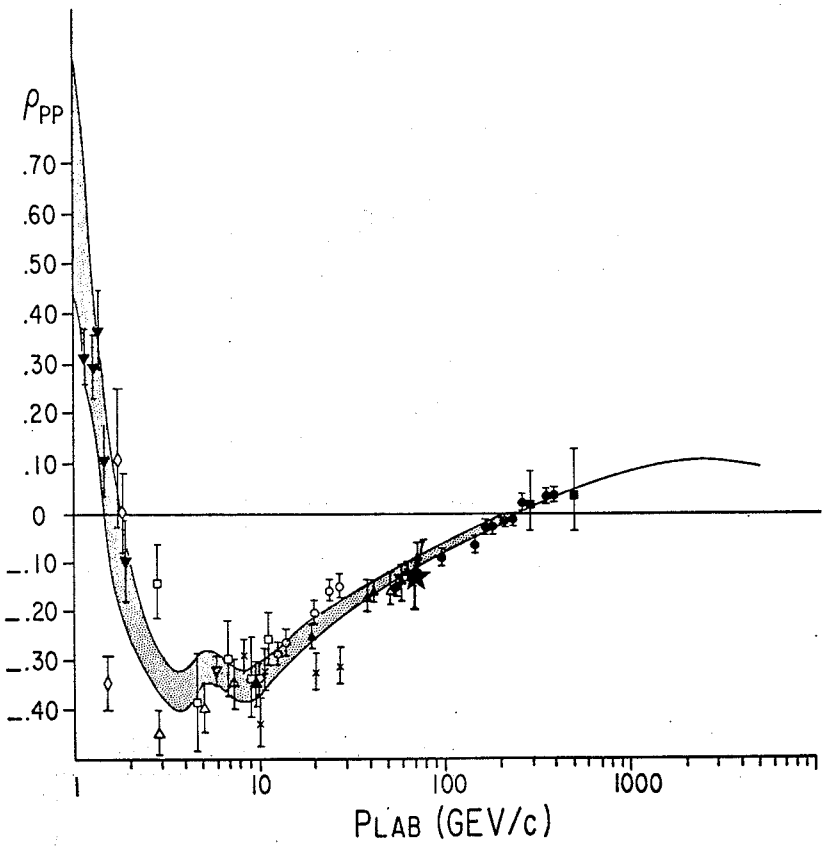
ρ_{PP}
.70
.60
.50
.40
.30
.20
.10
0
-.10
-.20
-.30
-.40
1
10
100
1000
PLAB (GEV/c)

Fig. 19

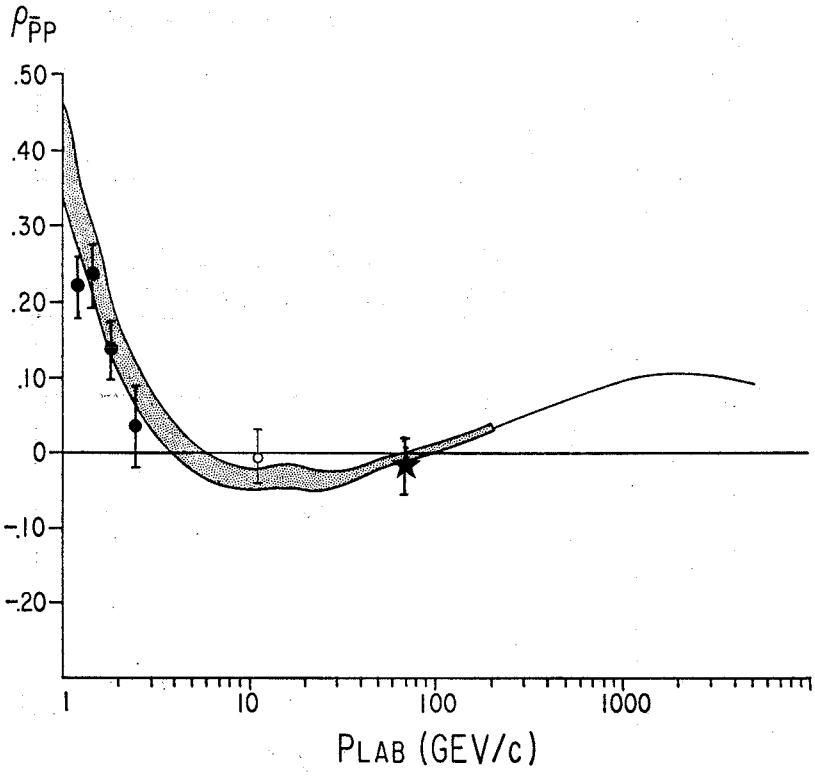
$\rho_{\bar{P}P}$
.50
.40
.30
.20
.10
0
-.10
-.20
1
10
100
1000
PLAB (GEV/c)

Fig. 20

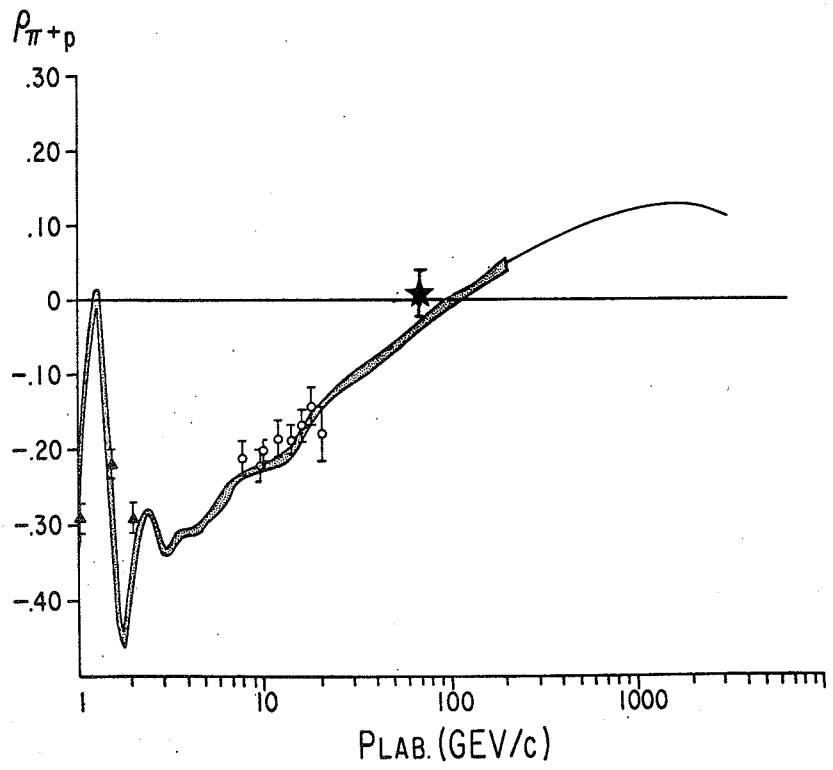
$\rho_{\pi^+ p}$
.30
.20
.10
0
-.10
-.20
-.30
-.40
1
10
100
1000
PLAB. (GEV/c)

Fig. 21

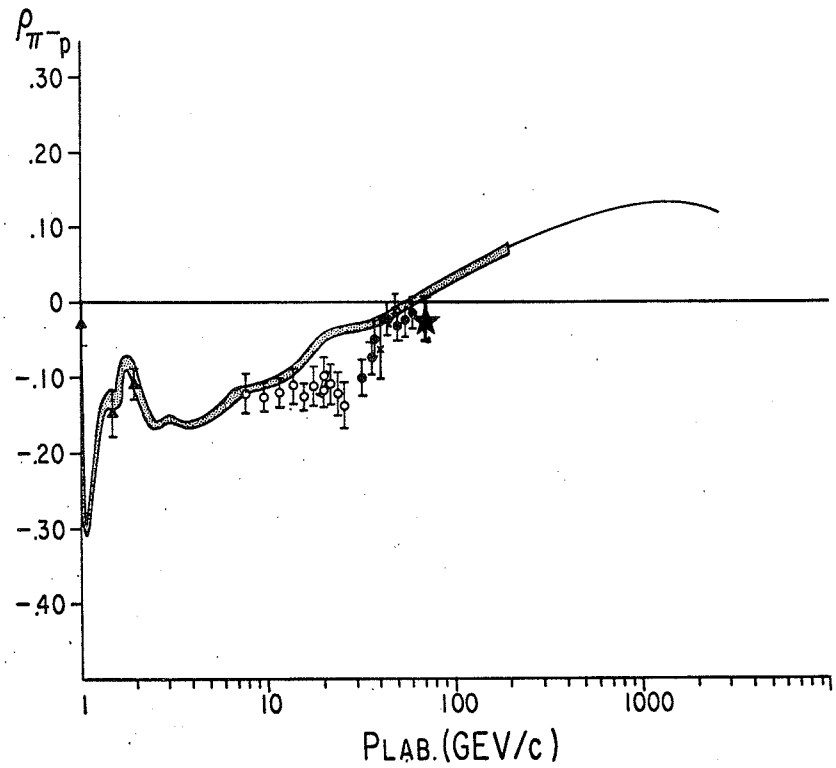
$\rho_{\pi^- p}$
.30
.20
.10
0
-.10
-.20
-.30
-.40
1
10
100
1000
PLAB. (GEV/c)

Fig. 22

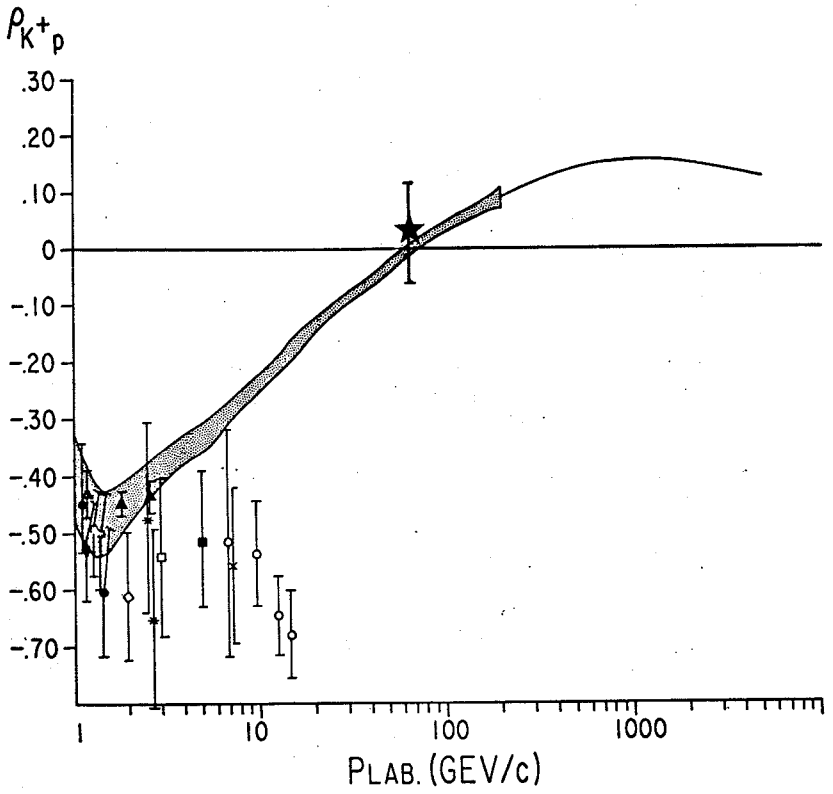
ρ_{K^+p}
.30
.20
.10
0
-.10
-.20
-.30
-.40
-.50
-.60
-.70
1
10
100
1000
PLAB. (GEV/c)

Fig. 23

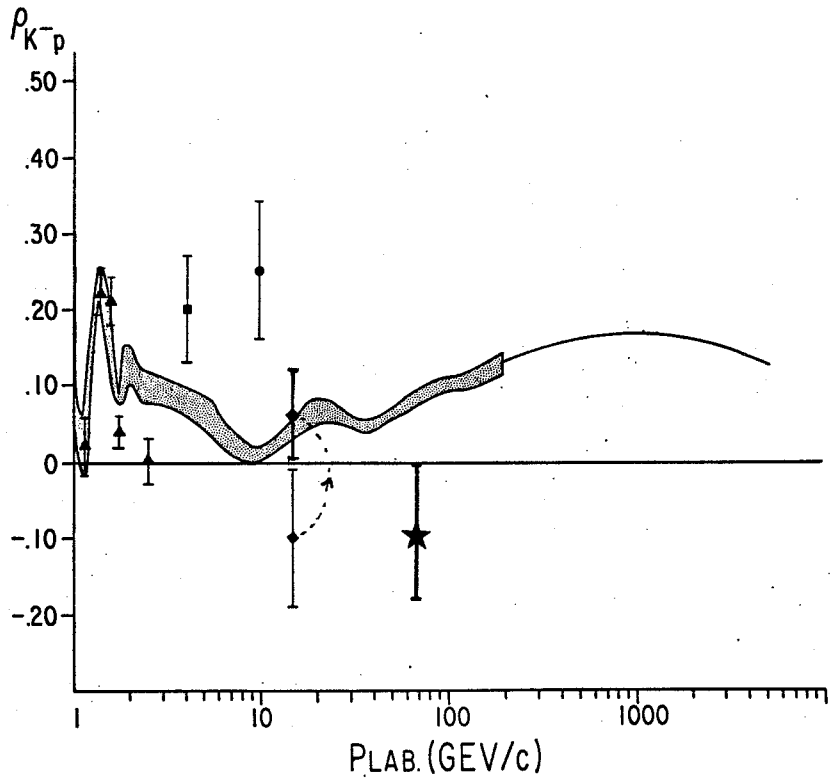
ρ_{K^-p}
.50
.40
.30
.20
.10
0
-.10
-.20
1
10
100
1000
PLAB. (GEV/c)

Fig. 24

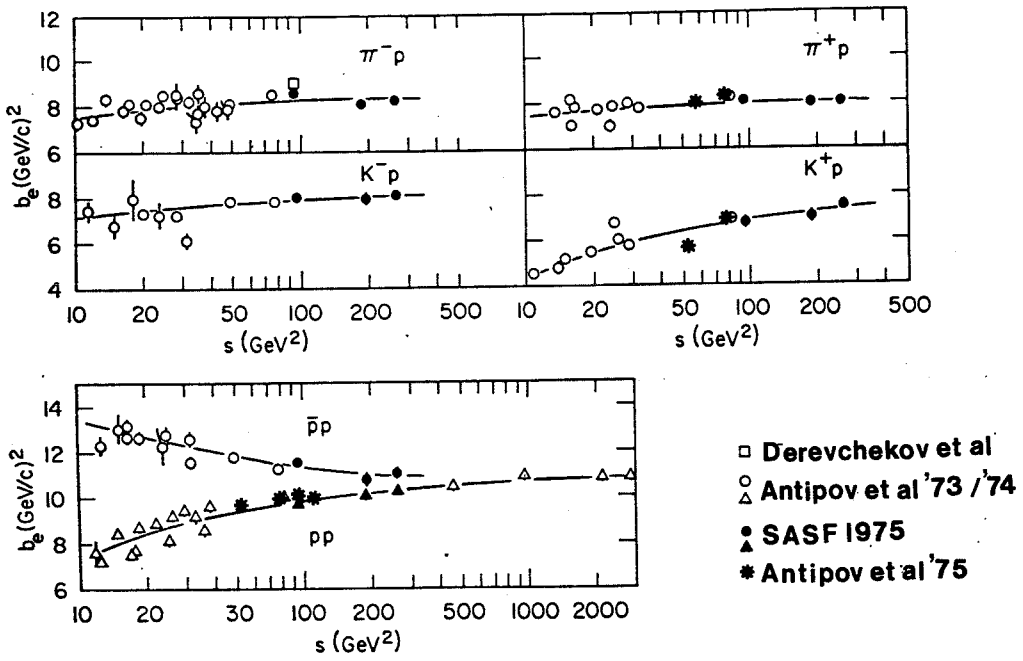
π^-p
π^+p
K^-p
K^+p
b_e(GeV/c)^2
s (GeV^2)
$\bar{p}p$
pp
□ Derevchekov et al
○ △ Antipov et al '73 /'74
● ▲ SASF 1975
✱ Antipov et al '75

Fig. 25

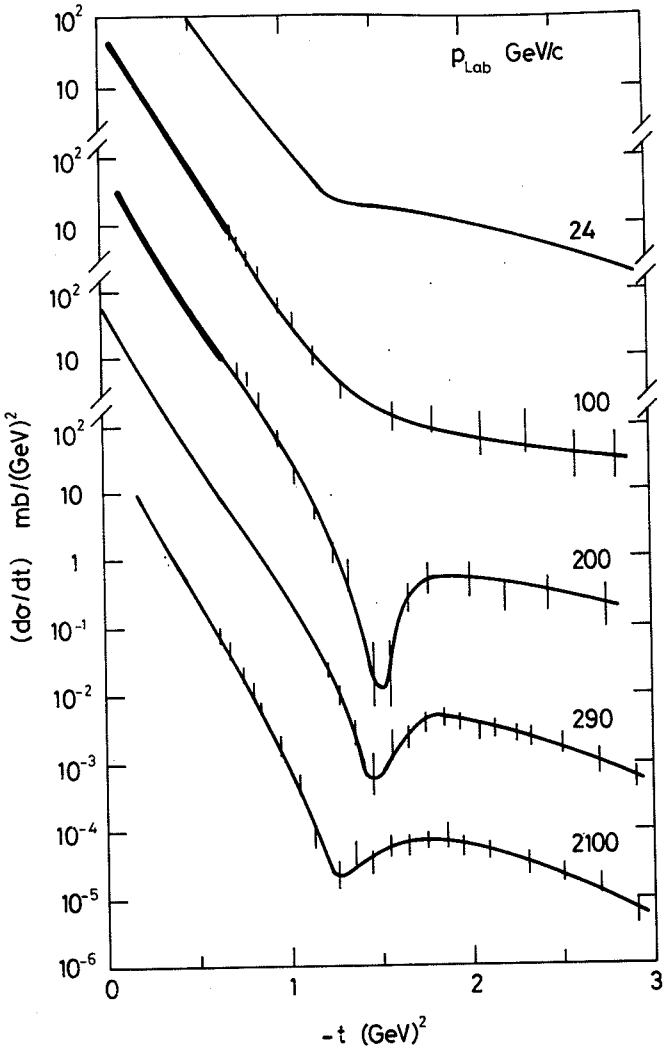
p_{Lab} GeV/c
24
100
200
290
2100
(do/dt) mb/(GeV)^2
-t (GeV)^2

Fig. 26

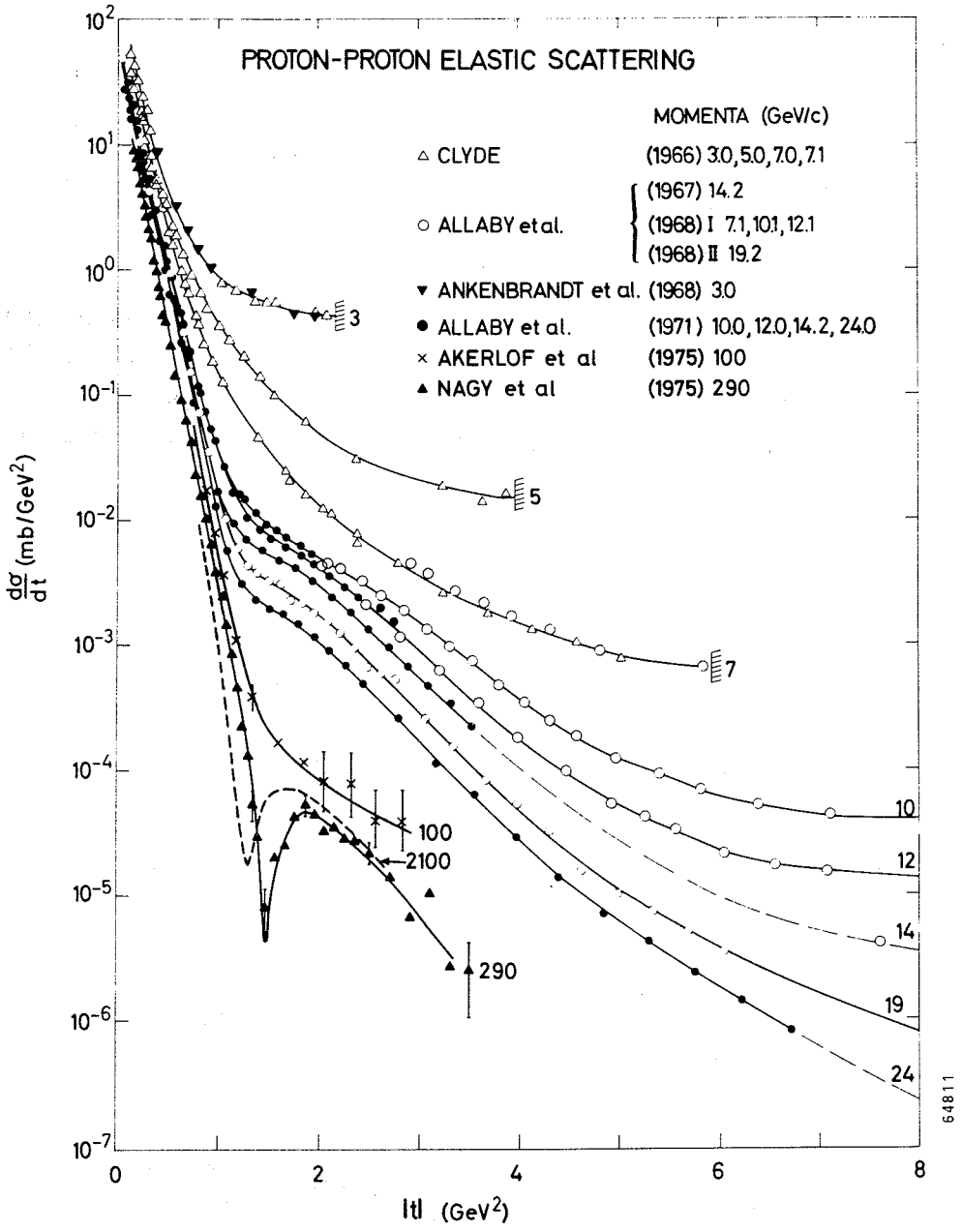
PROTON-PROTON ELASTIC SCATTERING
MOMENTA (GeV/c)
△ CLYDE (1966) 3.0, 5.0, 7.0, 7.1
○ ALLABY et al. (1967) 14.2
(1968) I 7.1, 10.1, 12.1
(1968) II 19.2
▼ ANKENBRANDT et al. (1968) 3.0
● ALLABY et al. (1971) 10.0, 12.0, 14.2, 24.0
× AKERLOF et al (1975) 100
▲ NAGY et al (1975) 290
3
5
7
10
12
14
19
24
100
2100
290
$\frac{d\sigma}{dt}$ (mb/GeV^2)
|t| (GeV^2)
64811

Fig. 27

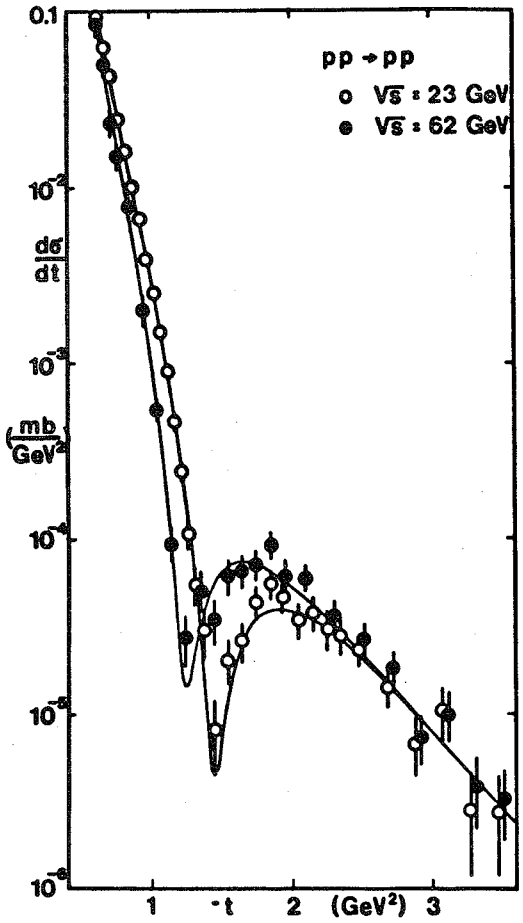
pp → pp
o √s = 23 GeV
● √s = 62 GeV
0.1
10⁻²
dσ/dt
10⁻³
(mb/GeV²)
10⁻⁴
10⁻⁵
10⁻⁶
1
-t
2
(GeV²)
3

Fig. 28

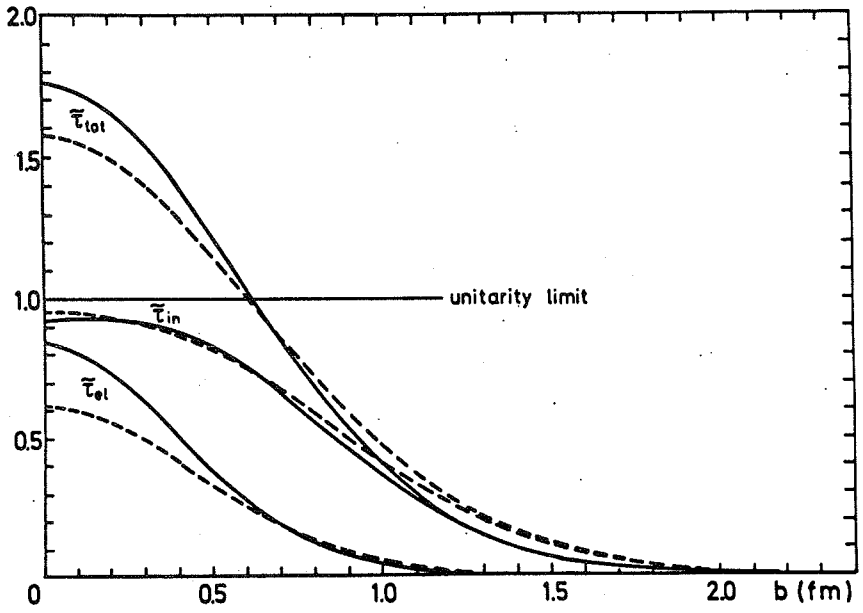
2.0
1.5
1.0
0.5
0
$\bar{\tau}_{tot}$
$\bar{\tau}_{in}$
$\bar{\tau}_{el}$
unitarity limit
0.5
1.0
1.5
2.0
b (fm)

Fig. 29

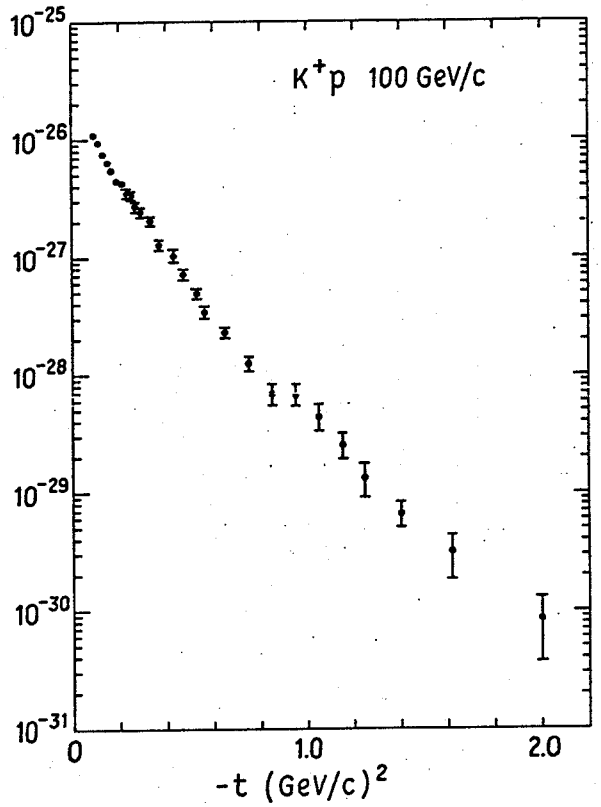
K^+p 100 GeV/c
10^{-25}
10^{-26}
10^{-27}
10^{-28}
10^{-29}
10^{-30}
10^{-31}
0
1.0
2.0
$-t\ (GeV/c)^2$

Fig. 30

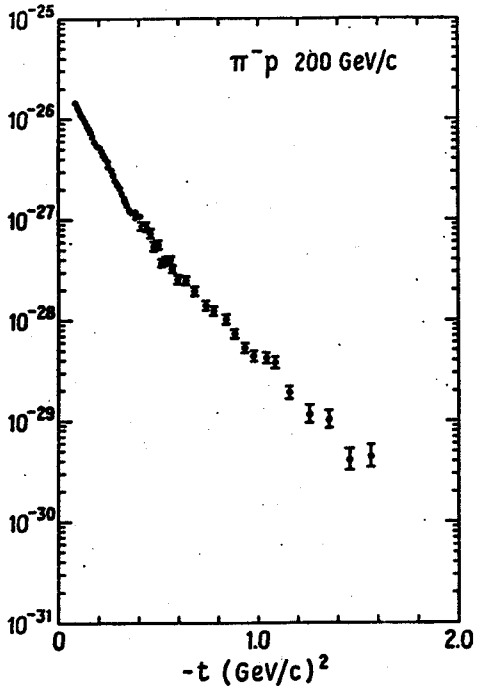
π^-p 200 GeV/c
10^{-25}
10^{-26}
10^{-27}
10^{-28}
10^{-29}
10^{-30}
10^{-31}
0
1.0
2.0
$-t\ (GeV/c)^2$

Fig. 31

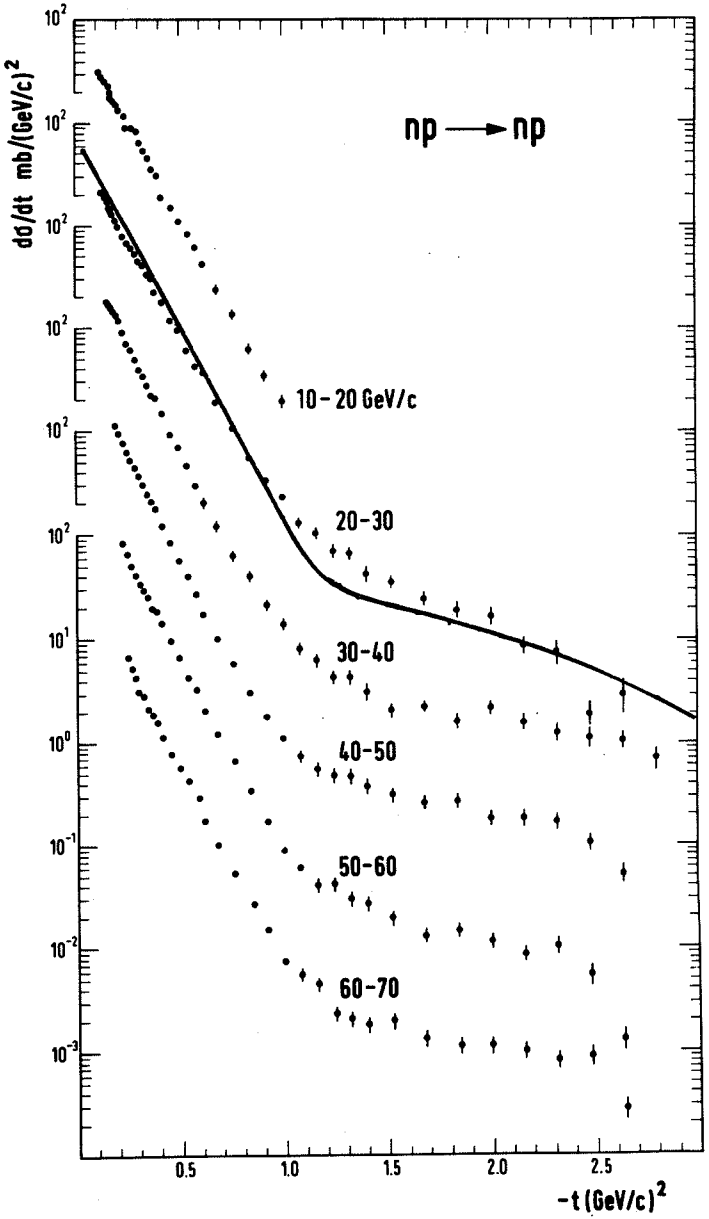
np → np
dσ/dt mb/(GeV/c)²
10-20 GeV/c
20-30
30-40
40-50
50-60
60-70
-t (GeV/c)²

Fig. 32

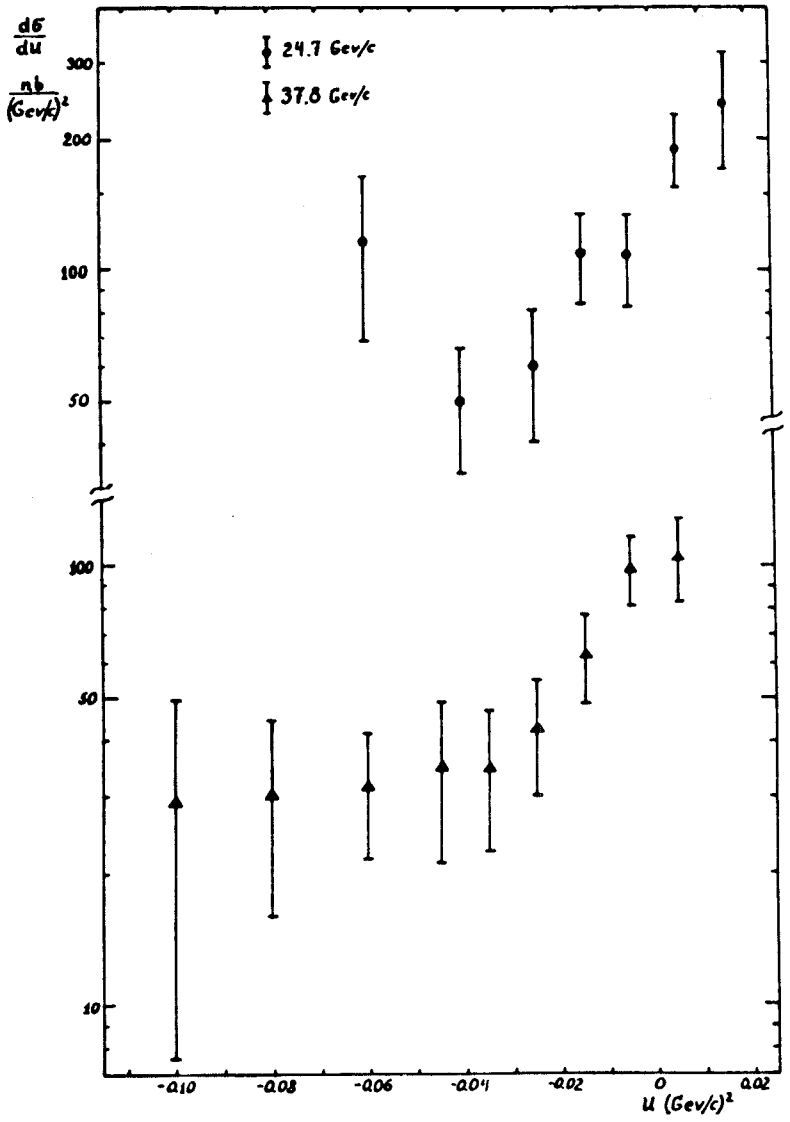
dσ/du
nb/(Gev/c)²
24.7 Gev/c
37.8 Gev/c
u (Gev/c)²

Fig. 33

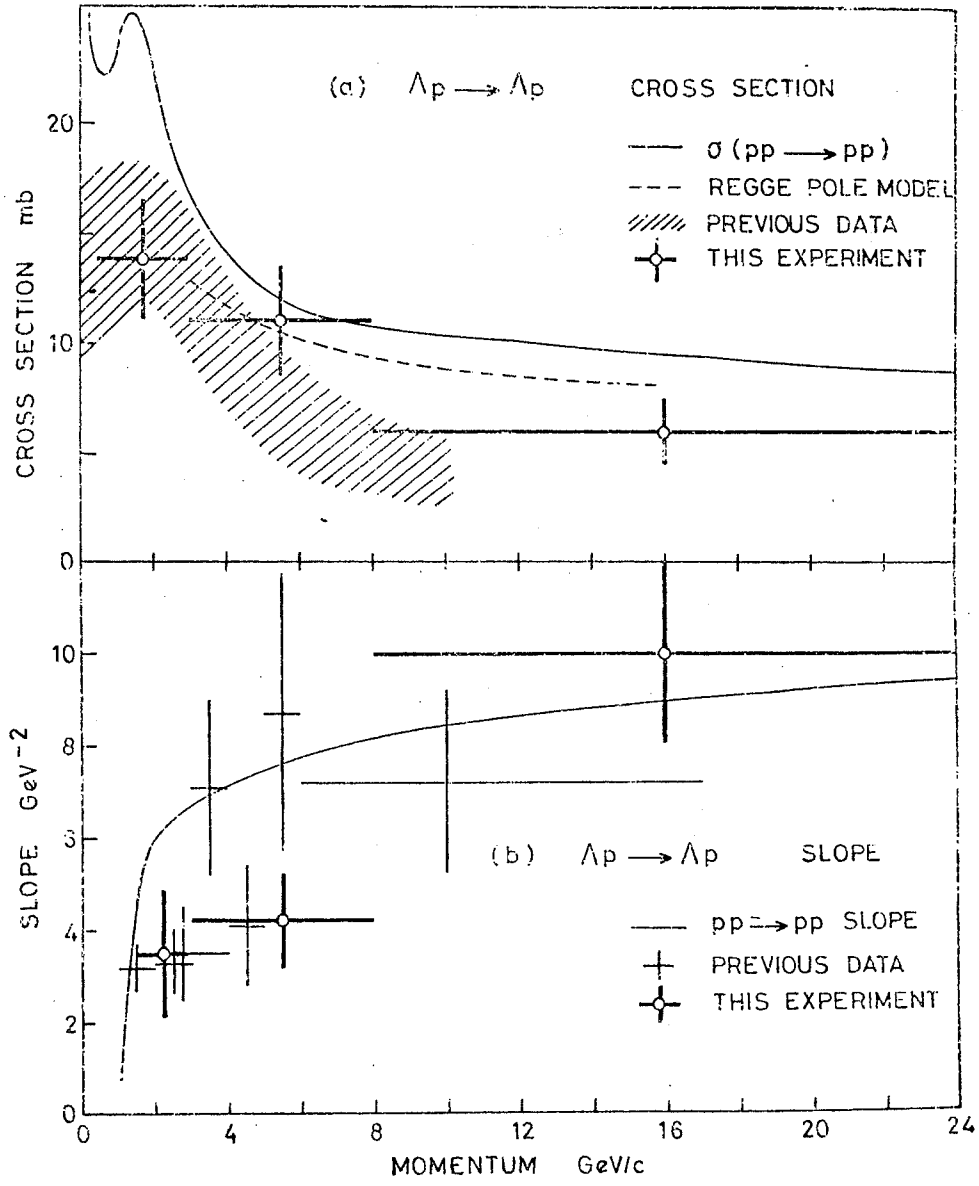
(a) Λp ⟶ Λp CROSS SECTION
σ (pp ⟶ pp)
REGGE POLE MODEL
PREVIOUS DATA
THIS EXPERIMENT
CROSS SECTION mb
(b) Λp ⟶ Λp SLOPE
pp ⟶ pp SLOPE
PREVIOUS DATA
THIS EXPERIMENT
SLOPE GeV⁻²
MOMENTUM GeV/c

Fig. 34

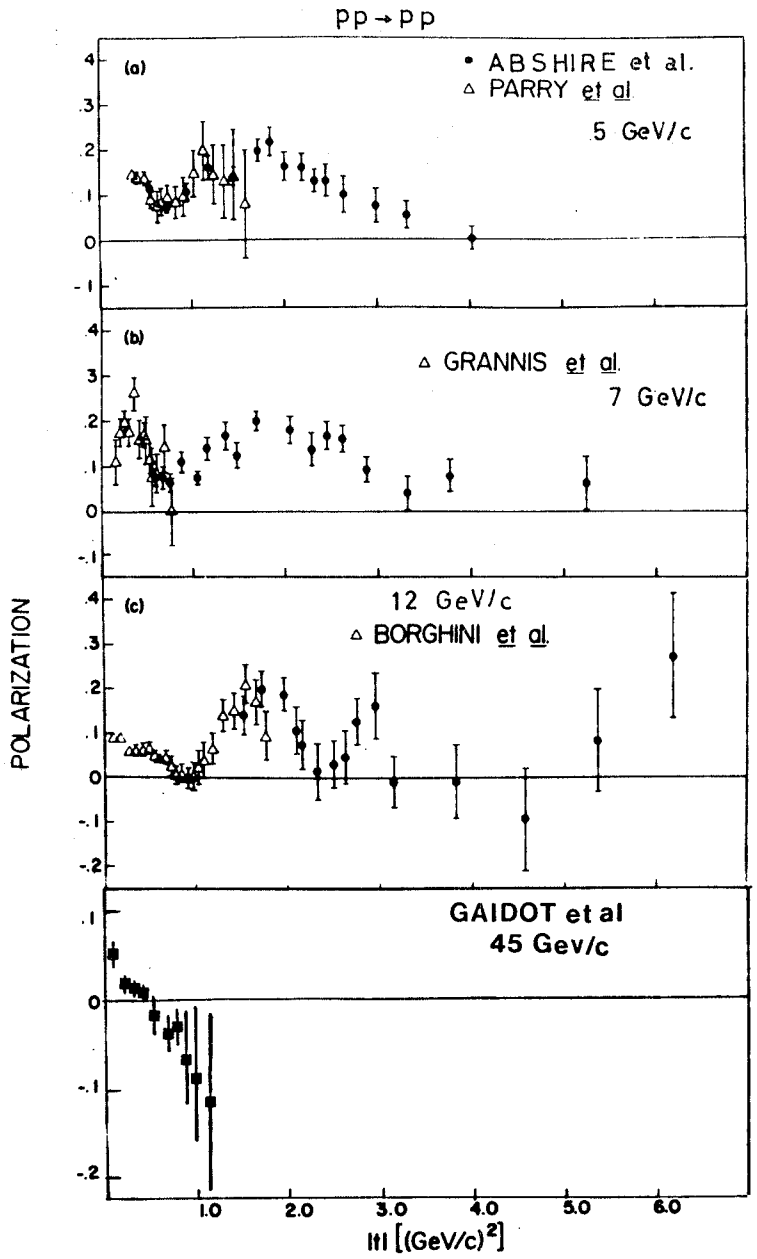
pp → pp
(a)
• ABSHIRE et al.
△ PARRY et al.
5 GeV/c
(b)
△ GRANNIS et al.
7 GeV/c
(c)
12 GeV/c
△ BORGHINI et al.
GAIDOT et al
45 Gev/c
POLARIZATION
|t| [(GeV/c)²]

Fig. 35

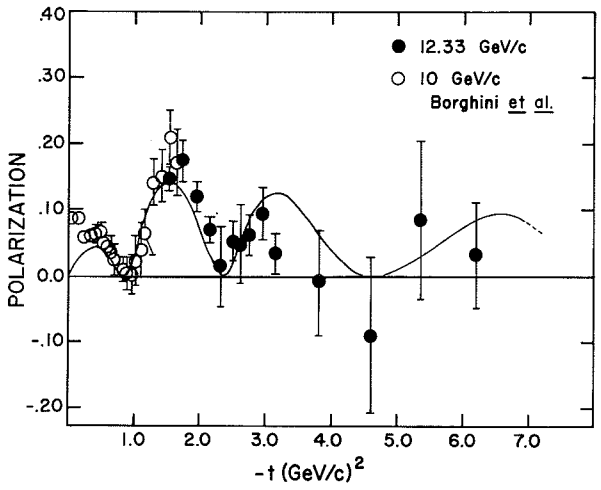
.40
.30
.20
.10
0.0
-.10
-.20
POLARIZATION
12.33 GeV/c
10 GeV/c
Borghini et al.
1.0
2.0
3.0
4.0
5.0
6.0
7.0
-t (GeV/c)²

Fig. 36

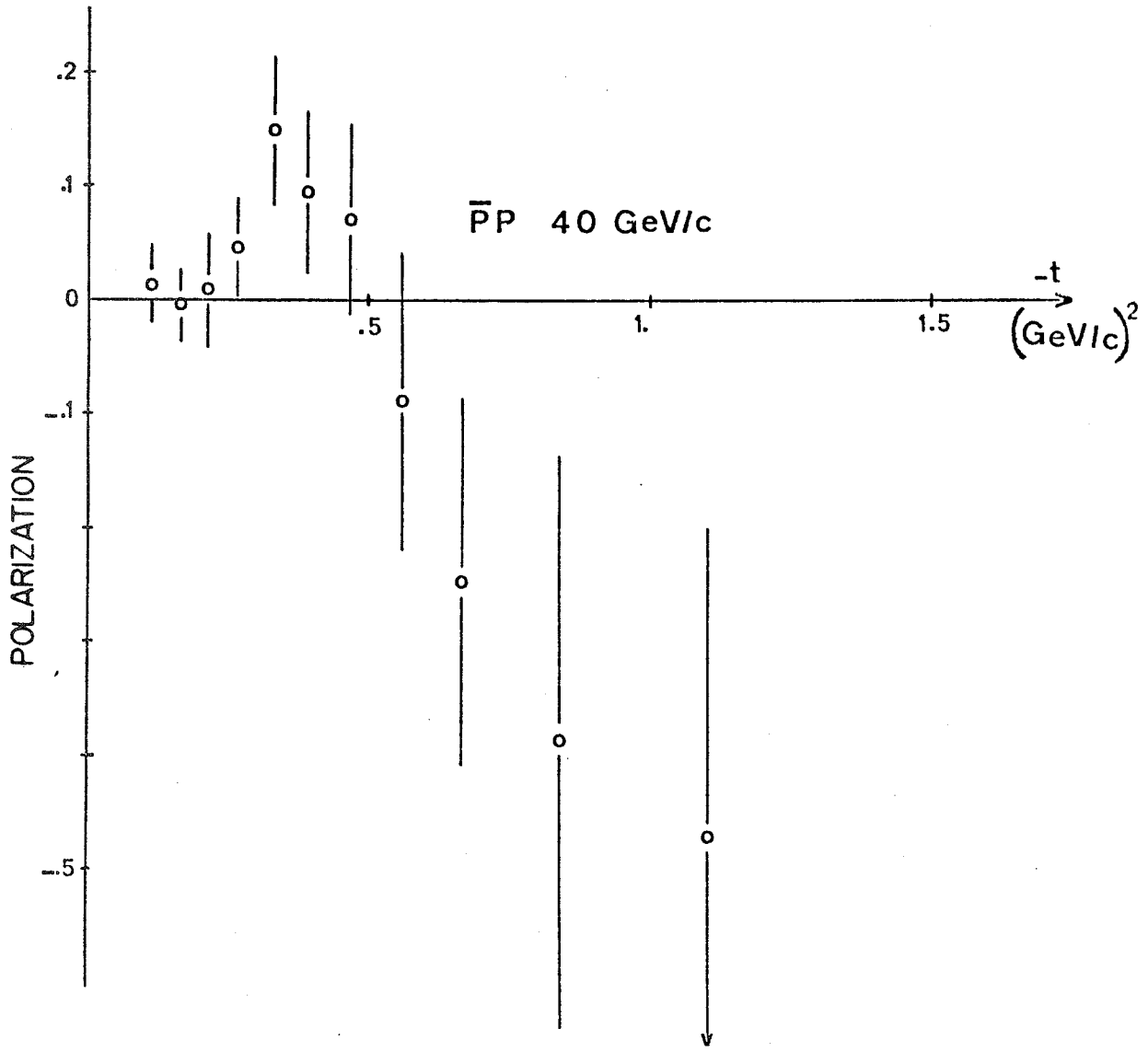
.2
.1
0
-.1
-.5
POLARIZATION
P̄P 40 GeV/c
-t
.5
1.
1.5
(GeV/c)²

Fig. 37

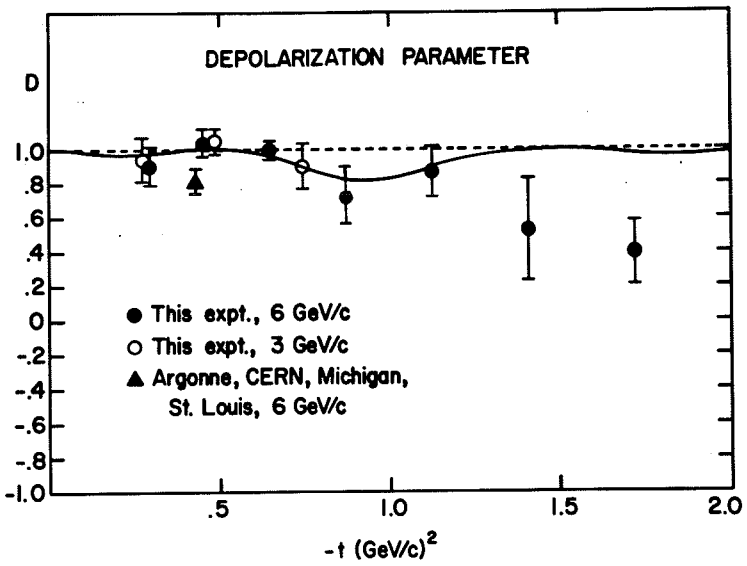
DEPOLARIZATION PARAMETER
D
1.0
.8
.6
.4
.2
0
-.2
-.4
-.6
-.8
-1.0
.5
1.0
1.5
2.0
● This expt., 6 GeV/c
○ This expt., 3 GeV/c
▲ Argonne, CERN, Michigan,
St. Louis, 6 GeV/c
-t (GeV/c)²

Fig. 38

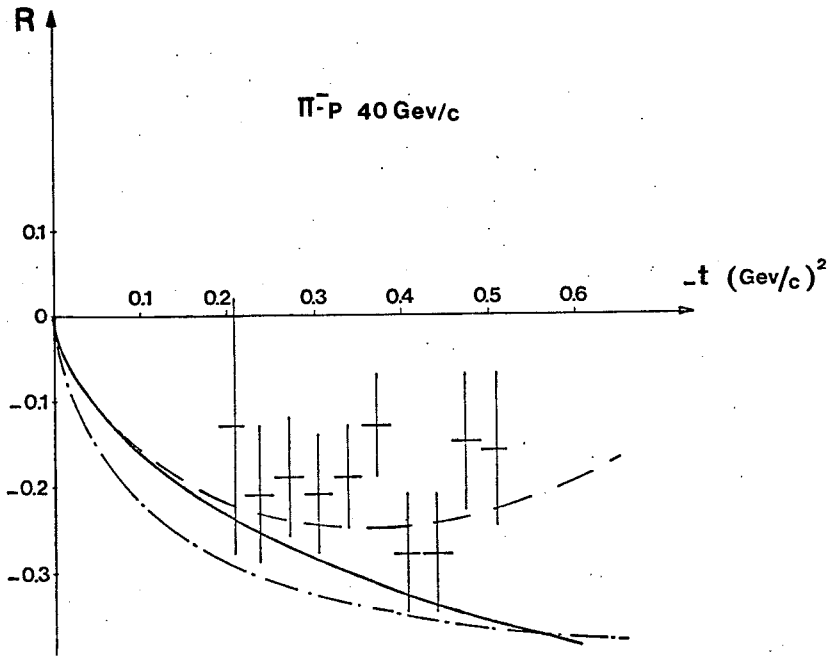
R
π⁻P 40 Gev/c
0.1
0
-0.1
-0.2
-0.3
0.1
0.2
0.3
0.4
0.5
0.6
-t (Gev/c)²

Fig. 39

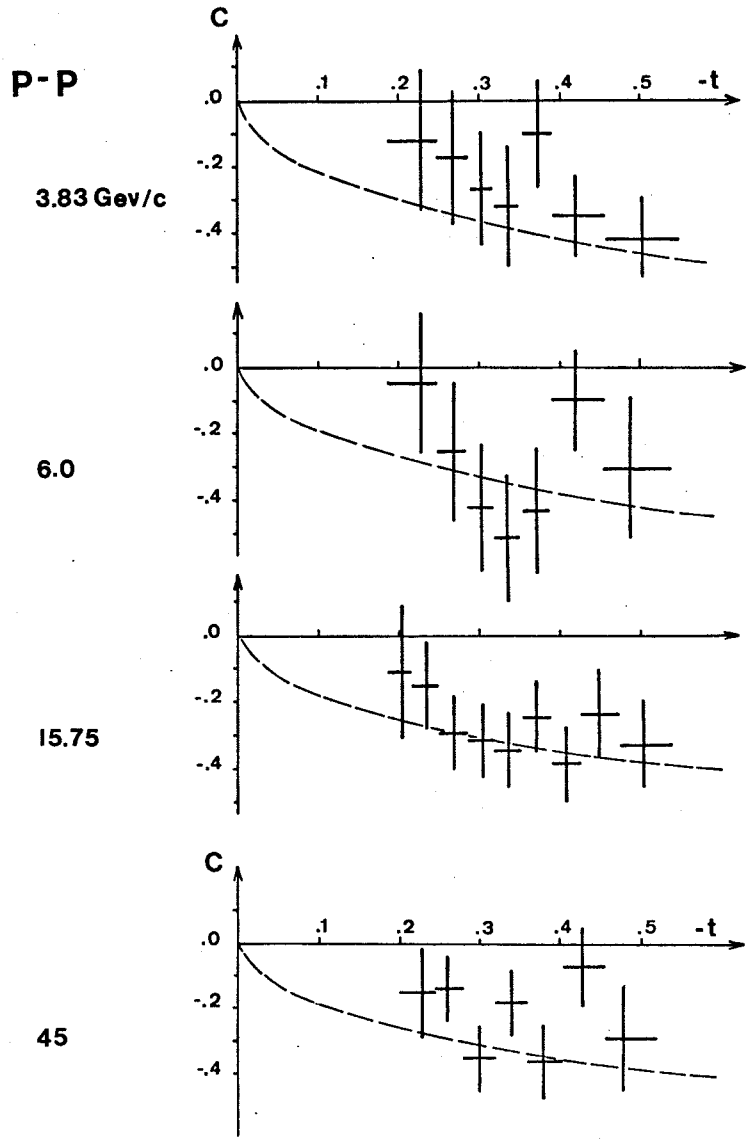
P-P
3.83 Gev/c
6.0
15.75
45
C
-t
.0
-.2
-.4
.1
.2
.3
.4
.5

Fig. 40

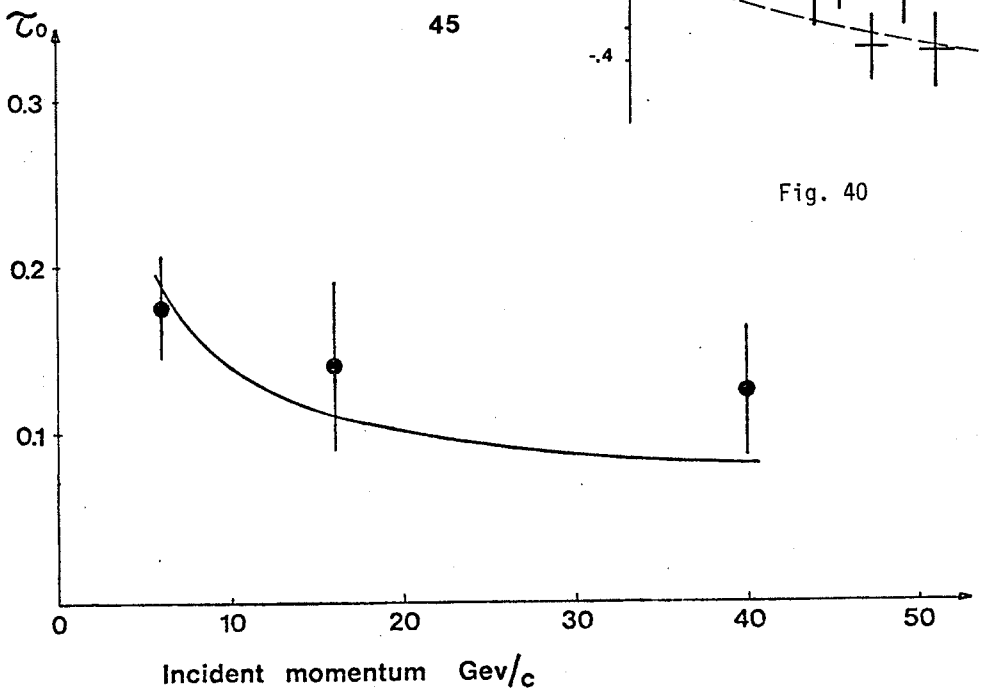
τ_0
0.3
0.2
0.1
0
10
20
30
40
50
Incident momentum Gev/c

Fig. 41

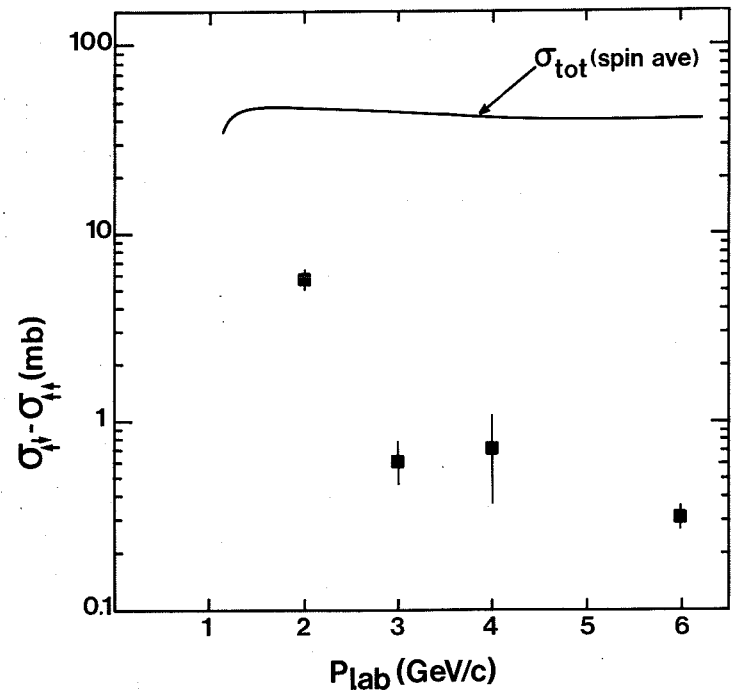
100
10
1
0.1
σ_{tot}(spin ave)
$\sigma_{\uparrow}$-$\sigma_{\uparrow\downarrow}$ (mb)
1
2
3
4
5
6
P_{lab} (GeV/c)

Fig. 42

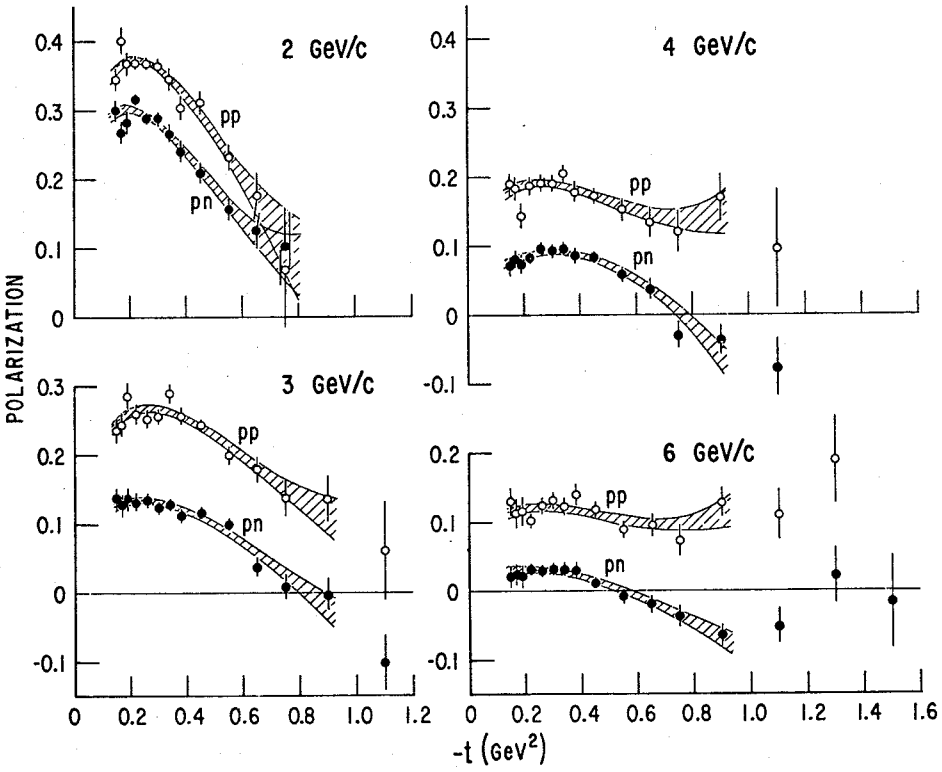
2 GeV/c
4 GeV/c
3 GeV/c
6 GeV/c
pp
pn
POLARIZATION
-t (GeV^2)

Fig. 43